

## Discovery of 2-[1-(4,4-Difluorocyclohexyl)piperidin-4-yl]-6-fluoro-3-oxo-2,3-dihydro-1*H*-isoindole-4-carboxamide (NMS-P118): A Potent, Orally Available, and Highly Selective PARP-1 Inhibitor for Cancer Therapy

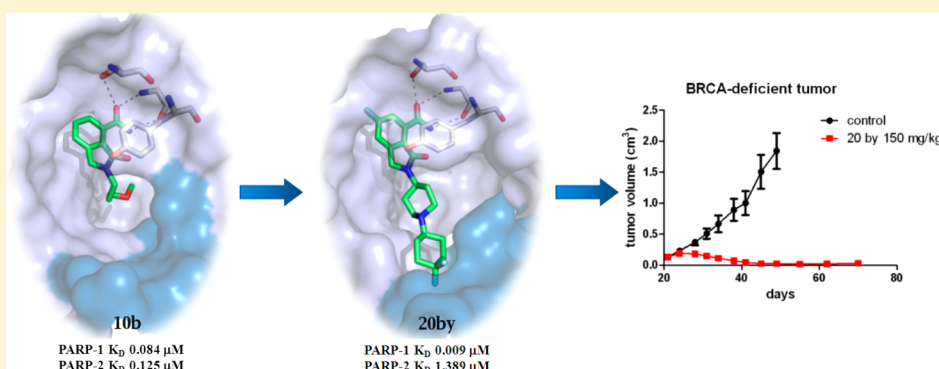
Gianluca Papeo,<sup>\*,†</sup> Helena Posteri,<sup>†</sup> Daniela Borghi,<sup>†</sup> Alina A. Busel,<sup>‡</sup> Francesco Caprera,<sup>†</sup> Elena Casale,<sup>†</sup> Marina Ciomei,<sup>†</sup> Alessandra Cirla,<sup>†</sup> Emiliana Corti,<sup>†</sup> Matteo D'Anello,<sup>†</sup> Marina Fasolini,<sup>†</sup> Barbara Forte,<sup>†</sup> Arturo Galvani,<sup>†</sup> Antonella Isacchi,<sup>†</sup> Alexander Khvat,<sup>‡,§</sup> Mikhail Y. Krasavin,<sup>‡,§</sup> Rosita Lupi,<sup>†</sup> Paolo Orsini,<sup>†</sup> Rita Perego,<sup>†</sup> Enrico Pesenti,<sup>†</sup> Daniele Pezzetta,<sup>§</sup> Sonia Rainoldi,<sup>†</sup> Federico Riccardi-Sirtori,<sup>†</sup> Alessandra Scolaro,<sup>†</sup> Francesco Sola,<sup>†</sup> Fabio Zuccotto,<sup>†,||</sup> Eduard R. Felder,<sup>†</sup> Daniele Donati,<sup>†</sup> and Alessia Montagnoli<sup>†</sup>

<sup>†</sup>Oncology, Nerviano Medical Sciences Srl, Viale Pasteur 10, 20014 Nerviano, Milan, Italy

<sup>‡</sup>Chemical Diversity Research Institute, Rabochaya St. 2 Khimki, Moscow Region 114401, Russia

<sup>§</sup>Accelera Srl, Viale Pasteur 10, 20014 Nerviano, Milan, Italy

### Supporting Information



**ABSTRACT:** The nuclear protein poly(ADP-ribose) polymerase-1 (PARP-1) has a well-established role in the signaling and repair of DNA and is a prominent target in oncology, as testified by the number of candidates in clinical testing that unselectively target both PARP-1 and its closest isoform PARP-2. The goal of our program was to find a PARP-1 selective inhibitor that would potentially mitigate toxicities arising from cross-inhibition of PARP-2. Thus, an HTS campaign on the proprietary Nerviano Medical Sciences (NMS) chemical collection, followed by SAR optimization, allowed us to discover 2-[1-(4,4-difluorocyclohexyl)piperidin-4-yl]-6-fluoro-3-oxo-2,3-dihydro-1*H*-isoindole-4-carboxamide (NMS-P118, **20by**). NMS-P118 proved to be a potent, orally available, and highly selective PARP-1 inhibitor endowed with excellent ADME and pharmacokinetic profiles and high efficacy *in vivo* both as a single agent and in combination with Temozolomide in MDA-MB-436 and Capan-1 xenograft models, respectively. Cocrystal structures of **20by** with both PARP-1 and PARP-2 catalytic domain proteins allowed rationalization of the observed selectivity.

### INTRODUCTION

The 113 kDa nuclear protein poly(ADP-ribose) polymerase-1 (PARP-1) is the most abundant and well-characterized member of the diphtheria toxin-like ADP-ribosyltransferase (ARTD) family of enzymes.<sup>1</sup> PARP-1 (aka ARTD-1) exerts its multi-faceted biological roles<sup>2,3</sup> through the construction of short-lived negatively charged ADP-ribose homopolymers [poly(ADP-ribose), PAR] either on PARP-1 itself (automodification) or on different acceptor proteins (heteromodification). Transferral of monomer units to the growing poly(ADP-ribose) chain

exploits the intermediacy of a reactive oxonium ion species which, in turn, arises from the PARP-1-catalyzed detachment of nicotinamide from nicotinamide adenine dinucleotide (NAD<sup>+</sup>).<sup>4</sup> The well-documented involvement of PARP-1 in the signaling and repair of DNA damage as well as its overactivation in several pathological contexts, triggered a number of aggressive medicinal chemistry programs aimed at the discovery of PARP-1 inhibitors,

**Received:** May 4, 2015

**Published:** July 29, 2015

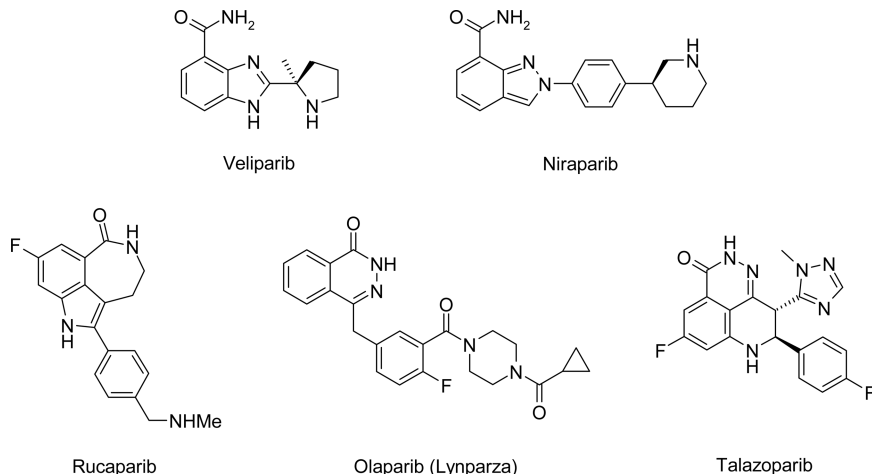


Figure 1. Examples of PARP inhibitors clinical candidates.

potentially useful in therapeutic areas as diverse as stroke, cardiac ischemia, diabetes, inflammation, and cancer.<sup>5</sup>

Presently, the primary focus of these efforts still concerns oncology, as testified by the tremendous amount of preclinical and clinical data produced in the field.<sup>6</sup> From a historical perspective, PARP-1 inhibitors entered the arena as promising coadjuvant components of standard chemo- and radiotherapy regimens. Later, the discovery that tumor cell lines bearing deficiencies or mutations in DNA-repair genes (e.g., BRCA1 or BRCA2) do not tolerate PARP-1 inhibition,<sup>7</sup> fuelled the application of PARP inhibitors as single-agent therapies in breast and ovarian BRCA-mutated cancer settings. More recently, the discovery of new potential combinative synergisms (e.g., PI3K<sup>8</sup>, NAMPT<sup>9</sup>, and EGFR<sup>10</sup> inhibitors) as well as the broadening of “synthetic lethality” contexts (e.g., PTEN<sup>11</sup> and ATM<sup>12</sup> mutations, MSI colorectal cancer phenotypes<sup>13</sup> and Ewing’s sarcomas<sup>14</sup>) in which the inhibition of PARP-1 can be therapeutically valuable has further raised interest in this target. Currently, eight PARP inhibitors are at different stages of clinical investigation, targeting several tumors types either in combination or as single agents.<sup>5</sup> These clinical candidates, as well as all known preclinical PARP-1 inhibitors, were designed to imitate the nicotinamide portion of NAD<sup>+</sup> with which they compete for the corresponding PARP-1 binding site. Accordingly, PARP-1 inhibitors are systematically endowed with two peculiar nicotinamide-mimic motifs: (1) a rotationally constrained primary amide as, for instance, in clinical candidates such as Veliparib (Abbott, Figure 1)<sup>15</sup> and Niraparib (Merck/Tesaro, Figure 1)<sup>16</sup> or (2) an amide embedded in a ring as in Rucaparib (Pfizer/Clovis, Figure 1),<sup>17</sup> Olaparib (AstraZeneca, now marketed as Lynparza, Figure 1),<sup>18</sup> and Talazoparib (BioMarin, Figure 1).<sup>19</sup> Within the PARP family of enzymes, none of these inhibitors selectively inhibits PARP-1. For instance, all the clinical candidates and the vast majority of reported PARP inhibitors also interact with PARP-2 (84% identity and 90% similarity within the PARP signature motif<sup>2,3a</sup>) with similar potencies, as recently independently described by Wahlberg<sup>20</sup> and ourselves.<sup>21</sup> PARP-2 (aka ARTD-2)<sup>1</sup> is a 62 kDa nuclear protein and, like PARP-1, is involved in DNA single-strand break repair. However, its contribution to the total DNA damage induced PARP activity is minimal (5–10%).<sup>22</sup> Specifically, PARP-2 has been postulated to participate in later steps of the DNA repair process by recognizing gaps and flaps and by the delayed and persistent accumulation at UV

laser-induced damaged sites.<sup>3</sup> Moreover, PARP-2 depleted cells show increased sensitivity to ionizing radiation, indicating a role in the IR induced DNA damage and suggesting a potential application for PARP-2 inhibitors in combination with irradiation.<sup>23</sup> Aside from PARP-1 and -2 overlapping functions, as clearly demonstrated by the embryonic lethality in double knockout mice, *PARP-2*<sup>-/-</sup> single knockout mice show impaired spermatogenesis, adipogenesis, and thymopoiesis. These *PARP-2*<sup>-/-</sup> mice furthermore suffer from increased neuronal loss after ischemic damage and are more prone to develop pancreatitis following chemical insult.<sup>22</sup> In addition, loss of PARP-2 has recently been shown to shorten erythrocytes lifespan and to impair differentiation of erythroid progenitors, leading to chronic anemia.<sup>24</sup> As all these physiological functions of PARP-2 can potentially result in undesirable side effects following its inhibition, we reasoned that a potent and highly selective PARP-1 inhibitor, if equally efficacious in cancer therapy as are dual PARP-1/-2 one, might represent a significant advancement in the field. Crucial data that prompted us to embark upon this strategy were the findings of Bryant<sup>7a</sup> and Sharp,<sup>25</sup> proving that PARP-1 genetic depletion is sufficient to induce death of BRCA2- and BRCA1-deficient tumor cell lines respectively, together with the feasibility of PARP-1 selective inhibitors (1 and 2 (BYK204165), Figure 2),<sup>26,27</sup> which were, however, designed for different therapeutic applications and did not progress to clinical testing.

Herein we describe the synthesis and SAR investigation of isoindolinone-4-carboxamide derivatives, leading to the discovery of 2-[1-(4,4-difluorocyclohexyl)piperidin-4-yl]-6-fluoro-3-oxo-2,3-dihydro-1*H*-isoindole-4-carboxamide (NMS-P118, 20by, Figure 2). NMS-P118 is a potent ( $K_D = 0.009 \mu\text{M}$ ) PARP-1 inhibitor, showing 150-fold selectivity over PARP-2 ( $K_D = 1.39 \mu\text{M}$ ). NMS-P118 possesses excellent pharmacokinetic profile and nearly complete oral bioavailability both in mice and rats. It proved to be highly efficacious in vivo both as single agent in MDA-MB-436 human breast cancer tumors and in combination with Temozolomide in Capan-1 human pancreatic tumors growing as xenografts in the mouse. The compound is well tolerated at highly efficacious doses and is endowed with an excellent ADME profile.

## ■ CHEMISTRY

Two synthetic pathways were exploited to access the planned isoindolinone-4-carboxamide derivatives. The first one capitalizes

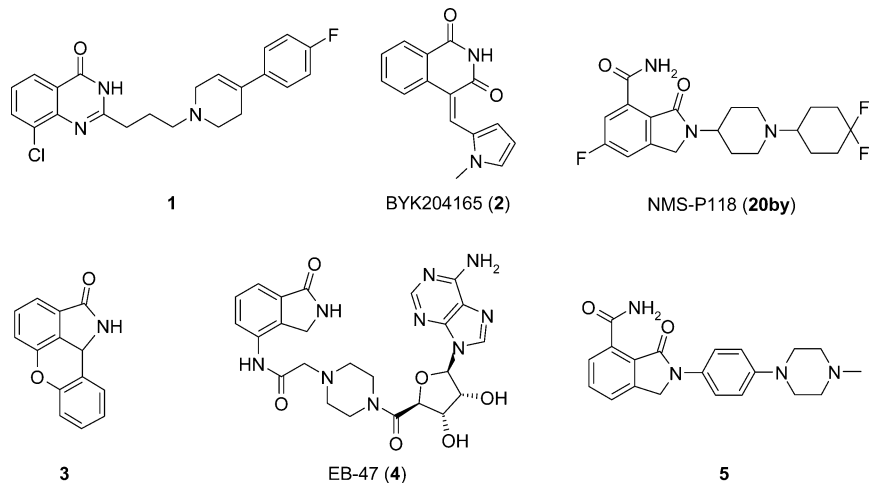
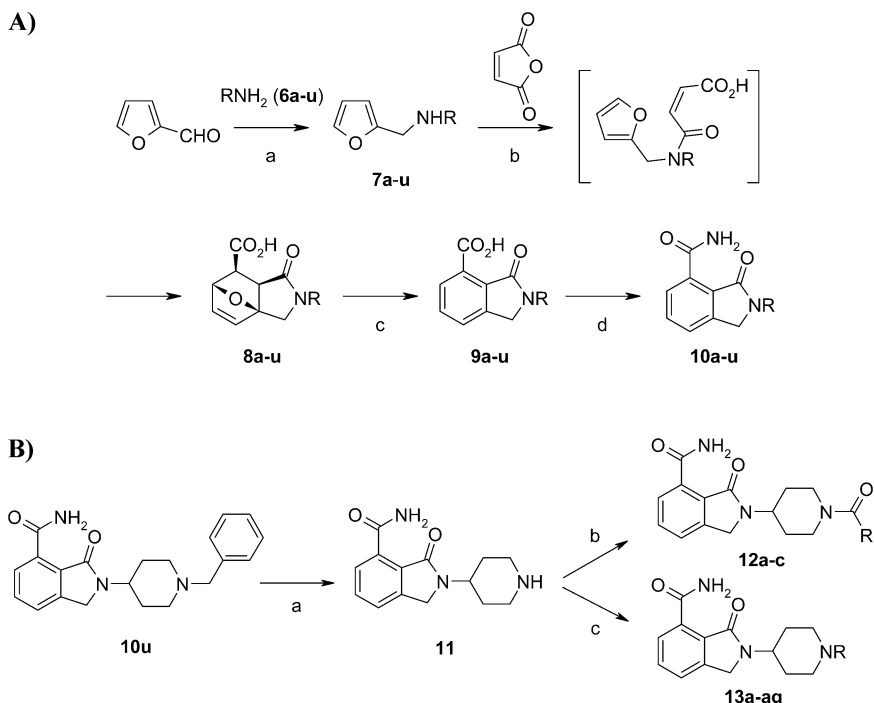


**Figure 2.** PARP-1 selective inhibitors (**1**, **2**), and NMS-P118 (**20by**) and isoindolinone-containing compounds (**3–5**).

**Scheme 1.** (A) Isoindolinones Synthesis via Intramolecular Diels–Alder Reaction;<sup>a</sup> (B) Elaboration of the piperidin-4-yl-moiety of intermediate **11**<sup>b</sup>

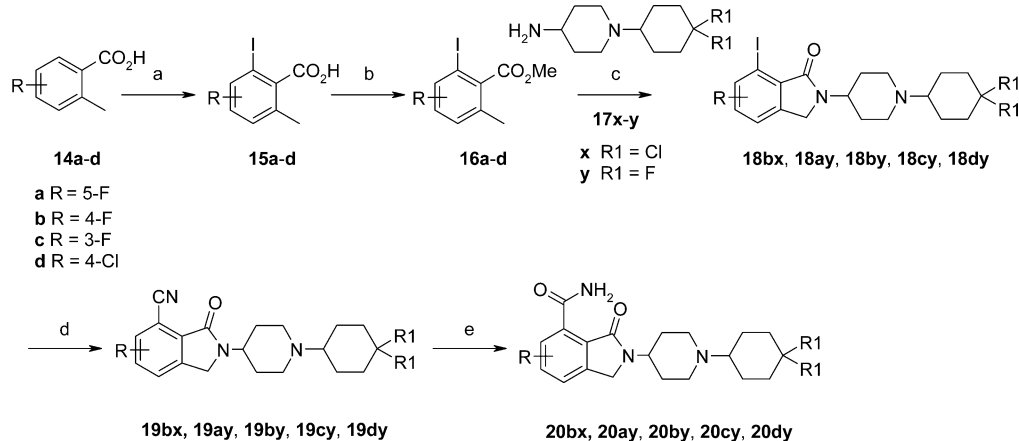


<sup>a</sup>Conditions: (a)  $\text{RNH}_2$  (**6**), dioxane or toluene (Dean–Stark), reflux then  $\text{NaBH}_4$ , ethanol, rt; (b) maleic anhydride, THF, rt or toluene, reflux; (c) concentrated aqueous hydrochloric acid, reflux; (d)  $\text{HOBr-NH}_3$ , EDCI-HCl, DIEA, DMF, rt. <sup>b</sup>Conditions: (a) 10% palladium on carbon, acetic acid, 50 psi, rt; (b)  $\text{RCOCl}$ , pyridine, 60 °C; (c) aldehyde or ketone,  $\text{CH}_3\text{COONa}$ ,  $\text{NaBCN}_3$  or  $\text{NaB(OAc)}_3\text{H}$ , dichloromethane/methanol, rt.

on an intramolecular Diels–Alder reaction as the key step (Scheme 1A).<sup>28</sup> Thus, furfural was initially subjected to a reductive amination protocol in the presence of suitable amines (**6a–u**) by preforming the Schiff bases which were then reduced with sodium borohydride. The corresponding properly functionalized furfurylmethylamines (**7a–u**) reacted with maleic anhydride in a two-step fashion by first delivering the transient maleic acid monoamide which then underwent an intramolecular Diels–Alder reaction. As anticipated,<sup>29</sup> the process is highly stereoselective, with only the *exo*-isomer being detected in the reaction mixture.

The *exo*-tricyclic adducts (**8a–u**) were then dehydrated by exposure to concentrated aqueous hydrochloric acid at reflux,

followed by conversion of the resulting carboxylic acids (**9a–u**) into the desired primary amides using the ammonium salt of hydroxybenzotriazole in the presence of EDCI as the coupling agent (**10a–u**). Despite the lack of a common intermediate, the synthetic sequence depicted in Scheme 1A is nonetheless straightforward because isoindolinone precursors (**7a–u**)–(**9a–u**) did not require any purification step. Further manipulation of the eastern portion of the isoindolinone core was achieved (Scheme 1B) by elaboration of the piperidin-4-yl-moiety of **11**<sup>30</sup> after debenzylation of **10u**. Compound **11** was then subjected to either acylation with acyl chlorides in pyridine or reductive alkylation in different conditions according to the carbonyl- counterpart, affording compound **12a–c** or **13a–ag**,

Scheme 2. Synthesis of Benzo-substituted Isoindolinone Derivatives 20<sup>a</sup>

<sup>a</sup> Conditions: (a) iodobenzene diacetate, I<sub>2</sub>, Pd(OAc)<sub>2</sub>, DMF, 100 °C; (b) methyl *p*-toluenesulfonate, K<sub>2</sub>CO<sub>3</sub>, DMF, rt; (c) N-bromosuccinimide, benzoyl peroxide, methyl pivalate, 85 °C, then 17x-y, triethylamine, acetonitrile, 90 °C; (d) CuCN, DMF, 110 °C; (e) acetaldoxime, InCl<sub>3</sub>, toluene, reflux.

respectively. To further investigate SAR within this chemical class, a second synthetic route to access benzo-substituted isoindolinone-4-carboxamide analogues was pursued (Scheme 2). The key step of this alternative approach is the *ortho* iodination of properly functionalized 2-methylbenzoic acids (14a–d) through C–H activation, as described by Yu et al.<sup>31</sup> Intermediates 15a–d were then transformed into the corresponding methyl esters 16a–d before being subjected to a radical bromination at the benzylic position. Crude benzyl bromides underwent a one-pot nucleophilic displacement–ring closure sequence<sup>28,30,32</sup> in the presence of easily accessible<sup>33</sup> amines (17x–y), thus yielding iodo-isoindolinone intermediates 18. A Rosenmund–von Braun protocol was subsequently applied to efficiently replace the iodine atom with a cyano group. Finally, the resulting isoindolinone-4-carbonitriles (19) were smoothly converted into the corresponding primary amides through a recently disclosed<sup>34</sup> indium(III) chloride-catalyzed transfer of water from acetaldoxime in refluxing toluene, producing compounds 20bx and 20(a–d)y.

## RESULTS AND DISCUSSION

By using our recently reported PARP-1 full length (FL) fluorescence polarization displacement assay,<sup>21</sup> a high throughput screening (HTS) campaign was conducted on the NMS proprietary chemical collection. Two isoindolinone-4-carboxamide derivatives (**10a** and **10b**, Table 1) emerged from this screening, possessing good biochemical activity on PARP-1 (each showing  $K_D = 0.09 \mu\text{M}$ ). The isoindolinone core is a known privileged scaffold for PARP inhibition,<sup>4</sup> either as a feature embedded within a tetracyclic structure (3, Figure 2)<sup>35</sup> or also, after appropriate linkage to adenosine, in NAD<sup>+</sup>-resembling compounds such as EB-47 (4, Figure 2).<sup>32</sup> Such inhibitors rely on the isoindolinone lactam moiety as a nicotinamide mimic. Subsequently, Abbott disclosed a series of 2-substituted isoindolinone-4-carboxamide derivatives (e.g., 5, Figure 2),<sup>30</sup> in which the carbonyl oxygen atom of the scaffold freezes the primary amide into its biologically active conformation through an intramolecular hydrogen bond, according to the alternative PARP-1 pharmacophore discussed above. All these compounds proved to be potent dual PARP-1/-2 inhibitors.<sup>21,30</sup>

The two low molecular weight compounds which emerged from our HTS campaign are highly efficient ligands<sup>36</sup> of PARP-1 (**10a**: MW = 218 Da, binding efficiency index (BEI) = 32.3,

ligand efficiency (LE) = 0.6; **10b**: MW = 248 Da, BEI = 28.4, LE = 0.54). Both compounds exhibited the desired mechanism of action in HeLa cells, i.e., both were able to inhibit PARP-1 dependent PAR synthesis in cells at micromolar concentrations following H<sub>2</sub>O<sub>2</sub>-induced DNA damage (PAR assay, Table 1). However, a fluorescence polarization displacement assay<sup>21</sup> using PARP-2 showed that both **10a** and **10b** also significantly bind this isoform (Table 1). Despite the moderate cellular activity and the lack of selectivity, the high intrinsic potency of these two hits deserved further investigation. The X-ray cocrystal structures of **10b** in complex with both human PARP-1 (hPARP-1, Figure 3A) and human PARP-2 (hPARP-2, Figure 3B) catalytic domains were solved in order to gain insight into the corresponding binding modes. As anticipated,<sup>30</sup> the pseudo seven-membered ring, arising from a  $\gamma$ -turn-like intramolecular hydrogen bond, locked the isoindolinone-4-carboxamide core into the *anti* conformation. This intramolecular interaction minimizes negative entropic contribution to the binding energy balance and allows **10b** to establish the usual network of hydrogen bonds within the proteins' catalytic domains (i.e., with Gly863 and Ser904 in hPARP-1 and with Gly429 and Ser470 in hPARP-2) and  $\pi$ -stacking (with Tyr907 in hPARP-1 and Tyr473 in hPARP-2) of a prototypical nicotinamide-mimic inhibitor.<sup>4</sup> To corroborate the presence of an intramolecular hydrogen bond not only in the crystal form, but also in solution, <sup>1</sup>H NMR spectra of **10b** in solvents with different polarity were recorded (Figure 4). The chemical shift difference ( $\Delta\delta = 3.08 \text{ ppm}$ ) between the downfield intramolecularly bonded amide proton and the upfield nonbonded one observed in a polar solvent such as DMSO-*d*<sub>6</sub> (Figure 4A) is fully consistent with this kind of interaction.<sup>37</sup> As expected, this difference was further exacerbated ( $\Delta\delta = 5.44 \text{ ppm}$ ) in a nonpolar solvent such as CDCl<sub>3</sub> (Figure 4B). These data were further consolidated by a quantitative assessment<sup>38</sup> of the intramolecular hydrogen bond strength (see Supporting Information (SI) for details). A closer inspection of the X-ray cocrystal structures of compound **10b** revealed that the methoxypropyl- side chain did not actively participate in binding of the inhibitor either to PARP-1 or to PARP-2, thus affording the possible opportunity of increasing PARP-1 potency by tailoring the substituent onto the lactam nitrogen atom. To this purpose, an overlay of cocrystal structures of **10b** and the selective quinazolinone inhibitor 1

Table 1. Isoindolinones Preliminary SAR Investigation

compd no.	R	PARP-1 K <sub>D</sub> (μM) <sup>a</sup>	PARP-2 K <sub>D</sub> (μM) <sup>a</sup>	PARP-2 K <sub>D</sub> / PARP-1 K <sub>D</sub> <sup>39</sup>	PAR IC <sub>50</sub> (μM) <sup>a</sup>
<b>10a</b>	-(CH <sub>2</sub> ) <sub>2</sub> CH <sub>3</sub>	0.084	0.422	5	1.14
<b>10b</b>	-(CH <sub>2</sub> ) <sub>3</sub> OCH <sub>3</sub>	0.087	0.125	1.4	5.30
<b>10c</b>	-(CH <sub>2</sub> ) <sub>2</sub> OCH <sub>3</sub>	0.220	-	-	-
<b>(±)-10d</b>		0.760	-	-	-
<b>10e</b>	-(CH <sub>2</sub> ) <sub>2</sub> OH	0.090	0.575	6.4	-
<b>10f</b>	-CH <sub>2</sub> C <sub>6</sub> H <sub>5</sub>	0.320	-	-	-
<b>10g</b>	-(CH <sub>2</sub> ) <sub>2</sub> C <sub>6</sub> H <sub>5</sub>	0.032	0.178	5.6	-
<b>10h</b>	-(CH <sub>2</sub> ) <sub>3</sub> C <sub>6</sub> H <sub>5</sub>	0.033	0.286	8.7	-
<b>10i</b>		< 0.030 <sup>b</sup>	< 0.030	1	-
<b>10j</b>		0.160	-	-	-
<b>10k</b>		0.035	5.870	168	2.15
<b>10l</b>		0.290	-	-	-
<b>10m</b>		< 0.030	3.360	> 112	0.20
<b>cis-10n</b>		0.330	-	-	-
<b>10o</b>		2.590	-	-	-
<b>10p</b>		0.049	0.670	14	-

Table 1. continued

compd no.	R	PARP-1 $K_D$ ( $\mu\text{M}$ ) <sup>a</sup>	PARP-2 $K_D$ ( $\mu\text{M}$ ) <sup>a</sup>	PARP-2 $K_D$ / PARP-1 $K_D^{39}$	PAR IC <sub>50</sub> ( $\mu\text{M}$ ) <sup>a</sup>
10q		0.056	0.420	7.5	-
10r		< 0.030	5.776	> 193	2.25
10s		0.031	1.112	36	-
10t		< 0.030	2.600	> 87	0.04
10u		0.050	> 10	> 200	2.00

<sup>a</sup> $K_D$  and IC<sub>50</sub> values are reported as the mean of 2–3 experiments. <sup>b</sup>Fluorescence polarization displacement assay sensitivity limit (see ref 21).

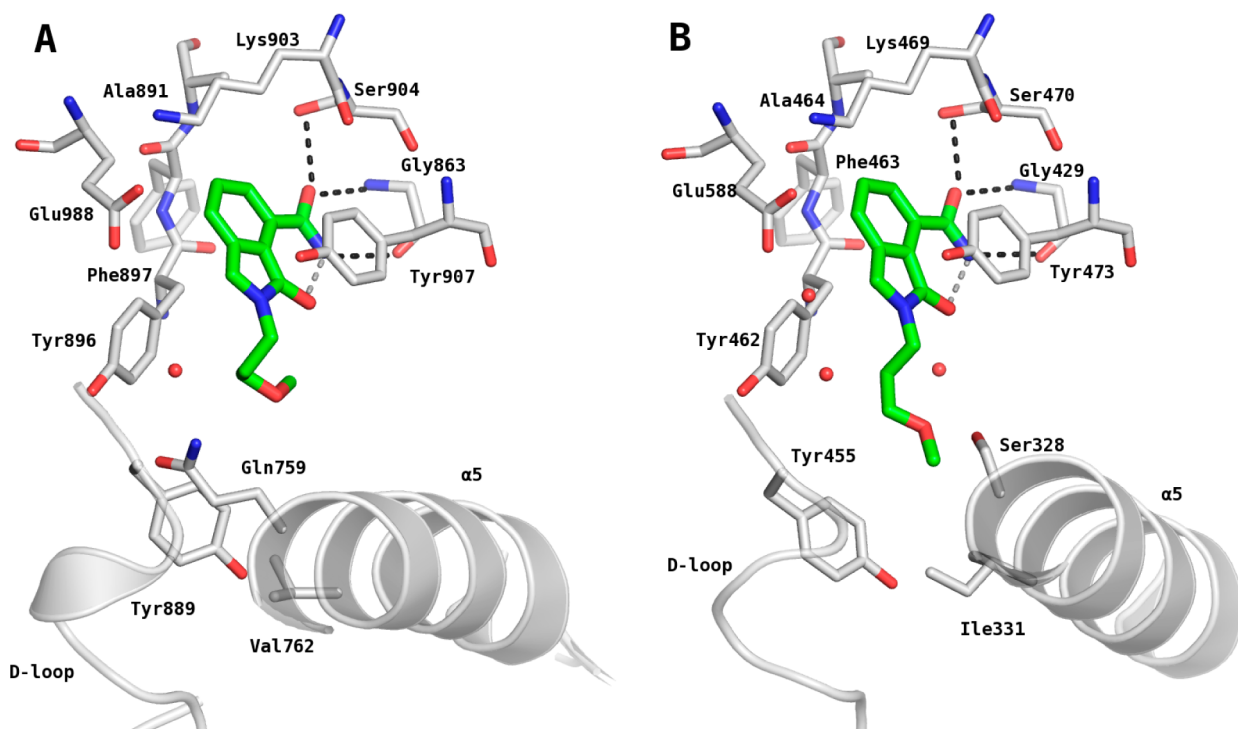
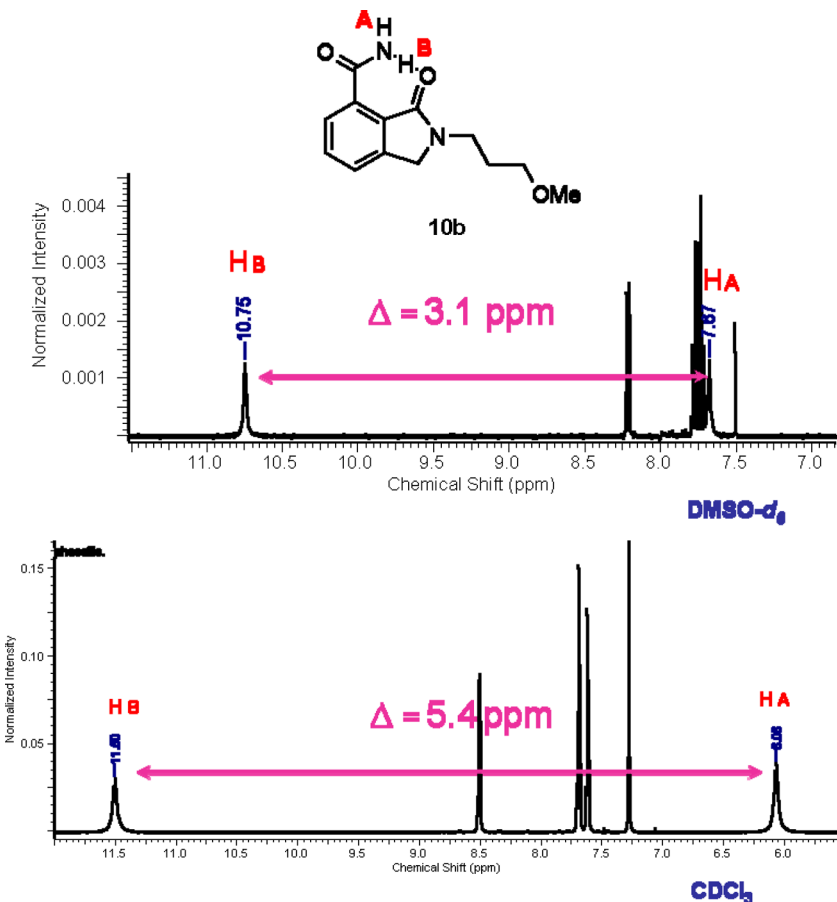


Figure 3. Cocrystal structures of **10b** with hPARP-1 (A) (PDB code 4ZZZ) and hPARP-2 (B) (PDB code 4ZZX) catalytic domain at 1.9 and 1.7 Å resolution, respectively.

(PDB code 1UK0) within hPARP-1 catalytic domain was analyzed (Figure 5). This exercise clearly ruled out the possibility to achieve selectivity against PARP-2 by engaging contacts within the adenine-ribose (AD) binding site,<sup>26a</sup> as the substituents departing from **10b** and **1** point at different

portions of the protein (see gray arrows in Figure 5). Nevertheless, compounds dramatically different in shape such as BYK204165 (2)<sup>27</sup> indicated that selectivity against PARP-2 might be achieved by targeting regions of the PARP-1 catalytic domain other than the AD site. Thus, a systematic exploration



**Figure 4.** Downfield portion of  $^1\text{H}$  NMR spectra of a 3 mM solution of **10b** in DMSO- $d_6$  (top) and CDCl<sub>3</sub> (bottom) showing the  $\Delta\delta$  of the two amide protons.

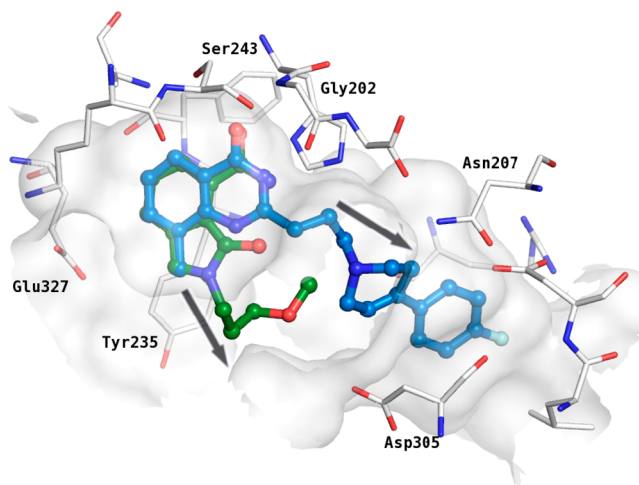


**Figure 5.** Overlay of cocrystal structures of **10b** (green carbon atoms, PDB code 4ZZZ) and quinazolinone **1** (light-blue carbon atoms, PDB code 1UK0) in the hPARP-1 binding site. Gray arrows indicate the direction of substituents departing from the nicotinamide-mimic scaffolds.

of this chemical class was undertaken alongside determination of compound selection criteria, based on biochemical potency (PARP-1  $K_D \leq 0.1 \mu\text{M}$ <sup>21</sup>) and selectivity (PARP-2  $K_D/\text{PARP-1 } K_D$  ratio of about 100<sup>39</sup>) thresholds. Inhibitors endowed with these features would then be tested to quantify their ability to suppress H<sub>2</sub>O<sub>2</sub>-induced PAR synthesis in HeLa cells, which

is exclusively PARP-1 dependent (PAR assay, see above). Derivatives possessing  $IC_{50} \leq 0.1 \mu\text{M}$  in this cellular assay would be considered eligible for preclinical profiling. Good oral bioavailability of the selected compounds was considered mandatory for further development.

After having established these cutoff criteria, HTS hits **10a** and **10b** were employed as a footprint to design a first array of isoindolinones. This set of compounds was assembled by varying: (a) the length of the aliphatic spacer connecting the nitrogen atom of the bicyclic core to the terminal eastern substituent and (b) the nature of the eastern substituent itself. Results are reported in Table 1. Thus, within the alkoxy-substituted series, shortening the spacer proved to be detrimental in terms of biochemical potency, regardless of whether the alkoxy group was linear or whether the oxygen atom was embedded in a cycle (compare **10c** and ( $\pm$ )-**10d** with **10b**). On the contrary, a hydroxyethyl substituent (**10e**) restored potency but did not possess PARP-1 vs PARP-2 selectivity. The biochemical activity of phenyl-substituted derivatives increased 1 order of magnitude upon going from benzyl (**10f**) to 2-phenylethyl (**10g**), with the latter being unacceptably potent also against PARP-2. A further elongation of the spacer (**10h**) impacted neither potency nor selectivity. By replacing the phenyl ring present in **10g** with a pyridin-2-yl moiety (**10i**), an increase in potency, mainly against PARP-2, was observed, with a  $K_D$  on both isoforms below the assay sensitivity limit.<sup>21</sup> By capitalizing on this result, we then investigated a series of isoindolinones encompassing differently substituted tertiary aliphatic amines located at a variable distance from the scaffold.

Table 2. In Vitro ADME Parameters and PK Data of Compound 10<sup>a</sup>

ADME parameters	PK parameters		
	10 mg/kg <sup>b</sup> IV administration	10 mg/kg <sup>b</sup> Oral administration	
solubility pH 7 ( $\mu\text{M}$ )	>225	$C_{\max}$ ( $\mu\text{M}$ )	4.9 $\pm$ 0.4
permeability PAMPA $P_{app}$ [ $10^{-6}$ cm/s] (% in membrane)	50.0 (20.8)	$AUC_{\infty}$ ( $\mu\text{M}\cdot\text{h}$ )	2.0 $\pm$ 0.2
PPB <sup>c</sup> (%)	98	CL (mL/min/kg)	230.0 $\pm$ 27.5
intrinsic CL (mL/min/kg) HLM <sup>d</sup>	14	$V_{ss}$ (L/kg)	3.4 $\pm$ 0.2
		$t_{1/2}$ (h)	0.2 $\pm$ 0.0
		F <sup>f</sup> (%)	nm <sup>e</sup>
			<1

<sup>a</sup>Harlan Nu/Nu mice;  $n = 3$  animals per study. <sup>b</sup>Dosed iv (intravenous administration), in situ prepared 10t hydrochloride in 5% dextrose; dosed per os (oral administration), 0.5% methocel. <sup>c</sup>Plasma protein binding. <sup>d</sup>Human liver microsomes. <sup>e</sup>nm: not measurable. <sup>f</sup>Bioavailability.

Both the morpholin-4-yl-ethyl- (10j) and the 1-piperidin-1-yl-ethyl- (10l) derivatives showed a lower potency against PARP-1 than the corresponding higher homologues (10k and 10m). Furthermore, compounds 10k and 10m showed, respectively, 160-fold and >110-fold selectivity toward PARP-1 over PARP-2 and were thus also profiled in the cellular PAR assay. While isoindolinone 10k showed no significant inhibition of PAR synthesis in cells, the IC<sub>50</sub> value of 10m, although modest, prompted us to further decorate the piperidinyl moiety in an effort to obtain more potent derivatives. The introduction of a 2,6-dimethyl substitution (*cis*-10n), as well as an additional piperidinyl ring (10o), resulted in a dramatic drop of activity. On the contrary, a lipophilic substituent such as a benzyl group in the 4 position of the piperidinyl ring (10p) restored the biochemical potency on both enzymes. The tetrahydroisoquinolin-2-yl-ethyl derivative (10r) proved to be more potent against PARP-1 and more selective toward PARP-2 than the corresponding isomeric tetrahydroquinolin-2-yl-ethyl substituted isoindolinone (10q). Unfortunately, 10r showed negligible activity in the cellular PAR assay. A further investigation was then conducted by moving the linker connecting the isoindolinone core to the piperidinyl ring from the 1 to the 4 position of the latter. The resulting derivatives were garnished with a lipophilic substituent onto the piperidinyl nitrogen atom, affording compounds 10s and 10t. While derivative 10s strongly inhibited PARP-1 but its selectivity toward PARP-2 was below our arbitrary threshold, the corresponding regiosomer 10t showed high biochemical potency on the target, excellent selectivity, and cellular activity.

Compound 10t was then subjected to in vitro ADME profiling and pharmacokinetic analysis in mice (Table 2). Disappointingly, despite the excellent solubility and good permeability, 10t showed high clearance in vivo (230 mL/min/kg) and negligible (<1%) oral bioavailability, thus preventing any further development. The preliminary SAR information emerged from this first cohort of isoindolinones underlines that a three- to four-carbon unit spacer between the bicyclic core and a basic center generally delivers the most potent and selective PARP-1 inhibitors. This observation prompted us to investigate the modulation of the potency and selectivity by embedding the spacer into a piperidine ring, whose nitrogen was initially decorated with a benzyl group (10u, Table 1). This lipophilic moiety was carefully chosen either because of its impact on the inhibitory activity within the series (see 10p, 10s, and 10t, Table 1) or because it can be easily replaced by standard chemistry (Scheme 1B). Compound 10u proved to be quite potent against PARP-1 and exceedingly selective. However, its ability in inhibiting the PARylation in cells was trifling (IC<sub>50</sub> = 2  $\mu\text{M}$ ). A second array of piperidin-4-yl substituted isoindolinones was then synthesized in order both to

implement the biochemical and cellular activity and the pharmacokinetic profile of the inhibitor. Results are reported in Table 3. The mandatory requirement of a basic nitrogen atom within this subseries was corroborated by the modest biochemical potency against PARP-1 of amide derivatives such as 12a–c. Linear or branched alkyl substituted piperidine (13a–e) delivered potent unselective compounds with flat SAR, while the presence of an oxygen atom within the aliphatic chain (13f) depressed the ability in inhibiting the target. More SAR information was gathered by playing around the initially selected benzyl substituent (10u). Thus, the introduction of a simple (electron donating) methyl substituent in the *ortho*, *meta*, and *para* position of the phenyl ring, respectively, afforded both biochemically potent and selective compounds (13g–i) whose enzymatic activity (13i = 13h > 13g) did not stringently mirror the cellular one (13i > 13g > 13h). Moderately deactivating groups such as bromine (13j–l) again confirmed the positive impact of a para substitution (13l) on both biochemical potency and selectivity, however, with no significant activity in cells. Strong electron withdrawing (13m–o) or donating (13p) groups generally worsened the inhibitor profile by delivering poorly active (13m), poorly selective (13o), or compounds lacking cellular activity (13n and 13p). The replacement of the phenyl ring with a pyridine (13q–s) produced potent and selective compounds and, in the case of the pyridin-2-ylmethyl derivative (13s), also with good (despite still suboptimal) cellular activity. Biochemically potent PARP-1 inhibitors also emerged by replacing the phenyl ring with a five-membered heterocycle such as thiophene (13t–u), furan (13v–z), and pyrrole (13aa–ab). However, the pair of compounds (13u and 13ab) which proved also to be selective against PARP-2 according to our screening criteria delivered disappointing results in PAR assay. Indole regiosomers (13ac–ad) behaved quite differently. While 13ac was not selective enough for further profiling, the potent and selective 5-substituted regiosomer (13ad) displayed an excellent cellular activity. Finally, few isoindolinones decorated with nonaromatic rings directly linked to the piperidine moiety (13ae–ag) were investigated. Despite being both potent and exceedingly selective, the 4,4-difluorocyclohexyl<sup>40</sup> substituted isoindolinone (13af) proved to be four times more active in cellular assay than the corresponding tetrahydro-2H-pyran-4-yl derivative (13ae). On the contrary, 1,3-dioxolane-containing compound 13ag showed only modest inhibitory activity against PARP-1. Having identified three compounds (13i, 13ad, and 13af) possessing the suitable biochemical potency, selectivity, and cellular activity, they were further profiled by analyzing their in vitro ADME and pharmacokinetic properties. Whereas permeability, plasma protein binding, and HLM clearance data were, on average, quite similar between the compounds,

Table 3. Piperidin-4-yl Substituted Isoindolinones SAR Investigation<sup>a</sup>

compd no.	R	PARP-1 K <sub>D</sub> ( $\mu$ M) <sup>b</sup>	PARP-2 K <sub>D</sub> ( $\mu$ M) <sup>b</sup>	PARP-2 K <sub>D</sub> / PARP-1 K <sub>D</sub> <sup>39</sup>	PAR IC <sub>50</sub> ( $\mu$ M) <sup>b</sup>
<b>10u</b>		0.050	> 10	> 200	2.00
<b>12a</b>		0.250	-	-	-
<b>12b</b>		0.150	-	-	-
<b>12c</b>		0.350	-	-	-
<b>13a</b>	-CH <sub>3</sub>	< 0.030 <sup>c</sup>	0.033	-	-
<b>13b</b>	-CH <sub>2</sub> CH <sub>3</sub>	< 0.030	0.340	-	-
<b>13c</b>	-CH(CH <sub>3</sub> ) <sub>2</sub>	< 0.030	0.075	-	-
<b>13d</b>	-CH <sub>2</sub> CH(CH <sub>3</sub> ) <sub>2</sub>	< 0.030	0.264	-	-
<b>13e</b>		< 0.030	0.441	-	-
<b>13f</b>	-(CH <sub>2</sub> ) <sub>2</sub> OCH <sub>3</sub>	0.113	-	-	-
<b>13g</b>		0.042	> 10	> 238	1.10
<b>13h</b>		< 0.030	8.714	> 290	9.90
<b>13i</b>		< 0.030	8.991	> 300	0.11
<b>13j</b>		0.034	6.916	203	> 10
<b>13k</b>		0.053	2.289	43	-

Table 3. continued

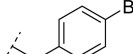
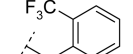
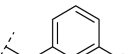
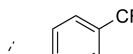
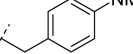
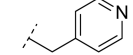
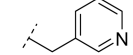
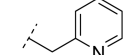
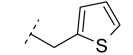
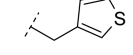
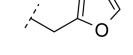
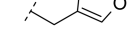
compd no.	R	PARP-1 K <sub>D</sub> ( $\mu$ M) <sup>b</sup>	PARP-2 K <sub>D</sub> ( $\mu$ M) <sup>b</sup>	PARP-2 K <sub>D</sub> / PARP-1 K <sub>D</sub> <sup>39</sup>	PAR IC <sub>50</sub> ( $\mu$ M) <sup>b</sup>
13l		< 0.030	2.425	> 81	6.00
13m		0.41	-	-	-
13n		0.046	> 10	> 217	3.00
13o		0.054	3.627	67	-
13p		0.039	> 10	> 256	6.60
13q		0.050	> 10	> 200	5.40
13r		0.072	6.804	> 95	13.40
13s		0.042	> 10	> 238	0.37
13t		< 0.030	1.435	-	-
13u		< 0.030	3.700	> 123	1.00
13v		< 0.030	1.698	-	-
13z		< 0.030	0.583	-	-
13aa		< 0.030	0.983	-	-
13ab		0.050	> 10	> 200	1.60

Table 3. continued

compd no.	R	PARP-1 K <sub>D</sub> (μM) <sup>b</sup>	PARP-2 K <sub>D</sub> (μM) <sup>b</sup>	PARP-2 K <sub>D</sub> / PARP-1 K <sub>D</sub> <sup>39</sup>	PAR IC <sub>50</sub> (μM) <sup>b</sup>
13ac		0.034	2.510	74	-
13ad		< 0.030	3.017	> 100	0.10
13ae		< 0.030	> 10	> 330	0.56
13af		< 0.030	3.937	> 131	0.15
13ag		0.132	-	-	-

<sup>a</sup>Intermediate 11 (Scheme 1B) was not tested as already reported not to be selective against PARP-2 (see ref 30 for details). <sup>b</sup>K<sub>D</sub> and IC<sub>50</sub> values are reported as the mean of 2–3 experiments. <sup>c</sup>Fluorescence polarization displacement assay sensitivity limit (see ref 21).

Table 4. In Vitro ADME Parameters of Selected Piperidin-4-yl Substituted Isoindolinones

compd no.	solubility pH 7 (μM)	permeability [10 <sup>-6</sup> cm/s] (% in membrane)	PAMPA P <sub>app</sub> PPB <sup>a</sup> (%)	CL (mL/min/kg) HLM <sup>b</sup>
13i	94	50.0 (31.0)	94	8
13ad	106	41.8 (36.1)	98	12
13af	> 225	28.8 (9.6)	85	7

<sup>a</sup>Plasma protein binding. <sup>b</sup>Human liver microsomes.

isoindolinone 13af showed a definitely higher solubility (Table 4). The PK profiles in mouse allowed selecting 13af as the lead compound of this isoindolinones subset (Table 5). In fact, while 13i was demonstrated to possess low oral bioavailability (15%), and 13ad, despite being orally available (80%), is rapidly cleared from the body (110 mL/min/kg), 13af proved to be suitable for oral administration (80%) with high exposure (21 μM·h) and low clearance (17 mL/min/kg). With the proper arrangement of the right end portion of the inhibitor in hand, a final medicinal chemistry refinement was undertaken in the attempt to further improve 13af cellular activity. The potency of 13af in PAR assay was indeed suboptimal (IC<sub>50</sub> = 0.15 μM). The planned optimization was focused on the preparation of a handful of compounds bearing small substituents on the phenyl ring of the isoindolinone bicyclic core, as the features of the back wall of PARP-1 hosting the nicotinamide moiety prevents the introduction of large groups.<sup>4</sup> The biochemical and cellular activities of this set of inhibitors are reported in Table 6.

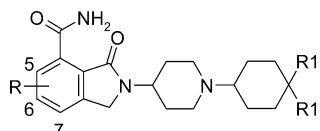
As none of the substituents introduced in the different positions of the aromatic ring are expected to deliver any steric clash within the catalytic site of the protein, SAR rationalization has to be found in the substituents' aptitude in modulating

the stereoelectronic properties of the inhibitors. Thus, the tremendous drop in biochemical activity of 20ay against PARP-1 was attributed to the loosening of the intramolecular hydrogen bond between the primary amide and the carbonyl oxygen by the fluorine atom in position 5. This effect can be appreciated by observing the small chemical shift differences between the two amide protons in the <sup>1</sup>H NMR spectra of 20ay (Table 7 and SI Table 1),<sup>37,38</sup> and is reasonably due to electron pair repulsion leading to conformational destabilization where the fluorine atom and the carbonyl are coplanar. A reduction in the intramolecular hydrogen bond strength, again measured as a decrease in the Δδ chemical shift between the two amide protons, might also account for the lower inhibitory activity displayed by the 7-fluoro isoindolinone 20cy compared to 13af (Table 7 and SI Table 1). On the other hand, in order to rationalize the high biochemical potency observed for both the 6-fluoro 20by and the corresponding 6-chloro derivative 20dy, additional interactions within the PARP-1 protein binding site were presumed (and later demonstrated, see below) to counterbalance the substituent's negative impact on hydrogen bond strength (Table 7 and SI Table 1). Because 20by was the most potent compound in PAR assay (IC<sub>50</sub> = 0.04 μM), the replacement of fluorine with chlorine atoms onto the cyclohexyl moiety<sup>41</sup> was then investigated by synthesizing compound 20bx (Table 6). Isoindolinone 20bx proved to be biochemically potent, selective against PARP-2 (as were all tested examples belonging to this subseries), and displayed an excellent activity in cells, thus demonstrating the importance of a properly 4-substituted cyclohexyl moiety to deliver PARP-1 inhibitors effective at a cellular level. To gain a deeper insight into 20by selectivity profile, the compound was tested against PARP-3 FL (aka ARTD-3; K<sub>D</sub> = 0.69 μM),<sup>21</sup> TNKS-1 catalytic domain (aka PARP-5a, ARTD-5; K<sub>D</sub> > 10 μM),<sup>21</sup> and sirtuin 1

**Table 5. PK Data of Selected Piperidin-4-yl Substituted Isoindolinones**

compd no.	PK data <sup>a</sup> iv						PK data <sup>a</sup> per os				
	dose <sup>b</sup> (mg/kg)	C <sub>max</sub> (μM)	AUC <sub>∞</sub> (μM·h)	CL (mL/min/kg)	V <sub>ss</sub> (L/kg)	t <sub>1/2</sub> (h)	dose <sup>c</sup> (mg/kg)	C <sub>max</sub> (μM)	AUC <sub>∞</sub> (μM·h)	t <sub>1/2</sub> (h)	F <sup>d</sup> (%)
13i	10	9.7 ± 0.9	8.2 ± 1.8	57.8 ± 13.0	2.2 ± 0.2	0.5 ± 0.1	10	1.1 ± 0.2	0.8 ± 0.2	nm <sup>e</sup>	15
13ad	4	2.0 ± 0.1	1.8 ± 0.9	110.0 ± 40.8	4.9 ± 0.8	0.7 ± 0.5	10	1.0 ± 0.3	3.7 ± 0.4	1.7 ± 0.6	80
13af	10	6.8 ± 0.6	26.3 ± 4.0	17.1 ± 2.5	3.4 ± 0.3	2.8 ± 0.1	10	3.6 ± 0.5	21.0 ± 3.1	2.9 ± 0.1	80

<sup>a</sup>Harlan Nu/Nu mice; n = 3 animals per study. <sup>b</sup>Dosed iv (intravenous administration): 5% Tween 80 in 5% dextrose for 13i, PEG 400 in 5% dextrose for 13ad, and 10% Tween 80 in 5% dextrose for 13af. <sup>c</sup>Dosed per os (oral administration): 0.5% methocel. <sup>d</sup>Bioavailability. <sup>e</sup>nm: not measurable.

**Table 6. SAR Investigation of Phenyl Substituted Isoindolinones**

compd no.	R	R1	PARP-1 K <sub>D</sub> (μM) <sup>a</sup>	PARP-2 K <sub>D</sub> (μM) <sup>a</sup>	PARP-2 K <sub>D</sub> / PARP-1 K <sub>D</sub> <sup>39</sup>	PAR IC <sub>50</sub> (μM) <sup>a</sup>
13af	H	F	<0.030 <sup>b</sup>	3.937	>131	0.15
20ay	S-F	F	1.880	—	—	—
20by	6-F	F	<0.030	2.500	>83	0.04
20cy	7-F	F	0.080	>10	>125	1.90
20dy	6-Cl	F	<0.030	>10	>333	0.50
20bx	6-F	Cl	<0.030	>10	>333	0.09

<sup>a</sup>K<sub>D</sub> and IC<sub>50</sub> values are reported as the mean of 2–3 experiments.

<sup>b</sup>Fluorescence polarization displacement assay sensitivity limit (see ref 21).

**Table 7. <sup>1</sup>H NMR Chemical Shifts Difference between Amide Protons of Selected Isoindolinones<sup>a</sup>**

compd no.	Δδ (ppm)
13af	3.07
20ay	0.24
20by	2.92
20cy	2.84
20dy	2.82

<sup>a</sup><sup>1</sup>H NMR spectra were recorded in DMSO-d<sub>6</sub> at 25 °C and 3 mM concentration.

(SIRT1; IC<sub>50</sub> > 10 μM). Because clinical PARP inhibitors, such as rucaparib and veliparib, show micromolar inhibitory activity also on some kinases,<sup>42</sup> compound 20by was also tested on a panel of 56 different kinases to assess its selectivity (IC<sub>50</sub> > 10 μM; see Experimental Section for details). Furthermore, to confirm the fluorescence polarization displacement assay data, 20by, along with 13af and the (unselective) 13c, were also

tested against PARP-1 and PARP-2 catalytic domain by surface plasmon resonance (SPR), an independent binding assay.<sup>21</sup> For comparative purposes, also the clinical candidates olaparib and veliparib (Figure 1) were tested in this assay.<sup>21</sup> SPR results are reported in Table 8. While 13c, as expected (Table 2), showed similar potency against both isoforms, isoindolinone 13af exhibits a PARP-1 K<sub>D</sub> = 0.016 μM and has approximately 75-fold less affinity for PARP-2. Finally, compound 20by proved to be a single-digit nanomolar PARP-1 inhibitor (K<sub>D</sub> = 0.009 μM), with exquisite selectivity versus PARP-2 (K<sub>D</sub> = 1.39 μM). Detailed kinetic parameters (SI Table 2) and kinetic analysis (SI Figure 1) of this assay can be found in the Supporting Information. The approximately 30% decrease in mere efficiency of binding (MW = 395 Da, BEI = 20.4, LE = 0.39), compared to the initial hits' efficiency (vide supra), underscores the fact that late stage optimization of 20by favored modifications contributing to the overall developability and bioactivity not just focusing on molecular binding interactions alone.

Compound 20by was tested along with 13af for the ability to inhibit proliferation of MDA-MB-436, a triple negative (HER2/ER/PR – ve) breast cancer cell line carrying BRCA1 gene mutation. The isoindolinone 20by resulted as being about 4 times more potent compared to 13af, with IC<sub>50</sub> of 0.14 and 0.6 μM, respectively, reflecting the higher target inhibition in PAR assay. Cellular models such as MCF-7 and MIA-PaCa-2 that do not have BRCA mutations or HR defects were resistant to both compounds with IC<sub>50</sub>s > 10 μM (Table 9). By aiming at rationalizing the high selectivity against PARP-2 showed by 20by, its X-ray cocrystal structures within the catalytic domains of hPARP-1 (Figure 6A) and hPARP-2 (Figure 6B) were solved. As expected, the contacts established by the isoindolinone-4-carboxamide core of 20by mirrored those of 10b (see Figure 3A,B). Additionally, the fluorine atom at position 6 fills a small cavity present in the binding sites of both proteins (defined by Phe897, Ala898, Lys903, and Glu988 residues in PARP-1 and by Phe463, Ala464, Lys469, and Glu558 residues in PARP-2) and interacts with the backbone carbonyl

**Table 8. K<sub>D</sub> Values and Dissociation Equilibrium Constants for PARP-1 and PARP-2 Catalytic Domain Determined with Biacore T-100**

compd no.	PARP-1 CD <sup>a</sup>			PARP-2 CD <sup>a</sup>		
	K <sub>D</sub> (μM) <sup>b</sup>	t <sub>1/2</sub> (min) <sup>b</sup>	K <sub>D</sub> (μM) <sup>b</sup>	t <sub>1/2</sub> (min) <sup>b</sup>		
olaparib	0.00024 ± 0.00012	51.12 ± 1.10	0.00028 ± 0.00013	17.40 ± 0.30		
veliparib	0.0017 ± 0.0003	1.53 ± 0.02	0.0058 ± 0.0004	1.10 ± 0.10		
13af	0.0157 ± 0.0005	1.68 ± 0.028	1.219 ± 0.305	0.07 ± 0.0006		
13c	0.075 ± 0.007	0.2 ± 0.06	0.118 ± 0.031	0.2 ± 0.068		
20by	0.0086 ± 0.0011	3.27 ± 0.11	1.389 ± 0.383	0.08 ± 0.0008		

<sup>a</sup>CD: catalytic domain. <sup>b</sup>Reported values are the average and standard deviation of three independent experiments.

**Table 9.** Antiproliferative Activity on Tumor Cell Lines<sup>a</sup>

compd no.	IC <sub>50</sub> ( $\mu$ M)		
	MDA-MB-436 (BRCA1 deficient)	MCF-7	MIA-PaCa-2
20by	0.14	>10	>10
13af	0.60	>10	>10

<sup>a</sup>Cells were exposed to different doses of the indicated compounds for 10–14 days, after which colonies were counted and IC<sub>50</sub> values were calculated.

of Phe897 in PARP-1 and Phe463 in PARP-2. The (4,4-difluorocyclohexyl)piperidinyl moiety points toward the donor loop and the  $\alpha$ -helical bundle domain, thus allowing the 4,4-difluorocyclohexyl ring to fill an induced pocket, to trigger the rearrangement of  $\alpha$ -helix 5 and to establish favorable hydrophobic interactions with a tyrosine residue of the donor loop (Tyr889 in PARP-1 and Tyr455 in PARP-2). The slightly dissimilar orientation of  $\alpha$ -helix 5 in the two proteins, together with the presence of different residues (Gln759 and Val762 in PARP-1 and Ile328 and Ser331 in PARP-2), may account for the selectivity observed, as the induced pocket is larger in PARP-1 (Figure 6A) than in PARP-2 (Figure 6B). As a result, the 4,4-difluorocyclohexyl substituent is better accommodated in PARP-1. The observation that  $\alpha$  helix 5 is intrinsically closer to the active site in PARP-2 than in PARP-1<sup>43</sup> further supports the hypothesis that the aforementioned rearrangement is energetically less favorable in PARP-2. To better characterize 20by, experiments of cross species metabolic stability in liver hepatocytes (SI Table 3), cytochrome P450 inhibition (SI Table 4), and in vitro myelotoxicity across species (SI Table 5), the latter in comparison with olaparib (Figure 1), were performed. Compound 20by proved to be metabolically stable, it modestly inhibited two cytochrome P450 family members (CYP-2B6 IC<sub>50</sub>, 8.15  $\mu$ M; CYP-2D6 IC<sub>50</sub>, 9.51  $\mu$ M) out of eight

isoforms tested. Its ability in hampering the proliferation of bone marrow cells was from 5 to >60 times lower than olaparib according to the species.

Overall, compound 20by appeared the most promising and was further progressed by evaluating its ADME and pharmacokinetic parameters in mouse, which proved to be excellent (Table 10). The compound showed high solubility and permeability, low in vitro and in vivo clearance, and complete oral bioavailability. The pharmacokinetic profile of 20by in rat dosed iv at 10 mg/kg and orally at 10 and 100 mg/kg (Table 10), mirrored that observed in the mouse, with oral bioavailability >65%, and linearity of exposure with dose.

To assess the in vivo antitumor activity of compound 20by when used as single agent, we treated nude mice bearing established subcutaneous MDA-MB-436 tumor xenografts (Figure 7). Oral administration of compound 20by for 28 days (once a day dose of 150 mg/kg) as a methocel suspension significantly inhibited tumor growth, inducing complete response (tumor impalpable) in all treated mice with no signs of toxicity or body weight loss. Six out of seven mice were still tumor free one month after the end of treatment.

We also examined the effect of combining 20by with Temozolomide in vivo. Tumor growth of subcutaneously implanted Capan-1 pancreatic xenografts was significantly inhibited when animals were treated by oral administration of 100 mg/kg 20by in combination with 50 mg/kg of Temozolomide. Even in the absence of significant antitumor activity for the two compounds given as single agent, 20by strongly potentiated Temozolomide, resulting in complete tumor regressions in 3 out of 6 animals (Figure 8). Only a slight increase in body weight loss was observed compared to the group treated with Temozolomide alone.

To assess the in vivo pharmacodynamics of 20by, Capan-1 xenograft-bearing mice received a single oral administration of

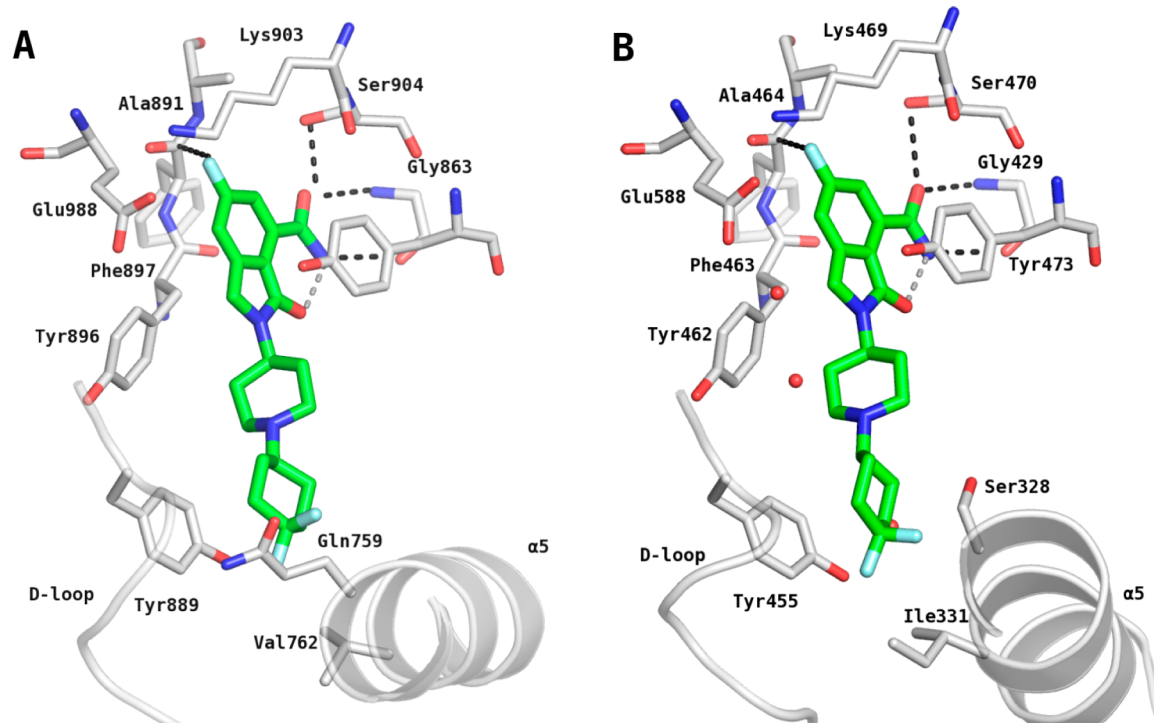


**Figure 6.** Cocrystal structures of 20by with hPARP-1 (A) (PDB code 5A00) and hPARP-2 (B) (PDB code 4ZZY) catalytic domain at 2.7 and 2.2  $\text{\AA}$  resolution, respectively.

Table 10. In Vitro ADME Parameters and PK Data of Compound 20by

ADME parameters		PK parameters					
		mouse <sup>a</sup>		rat <sup>b</sup>			
		iv <sup>c</sup> 10 mg/kg	oral <sup>c</sup> 10 mg/kg	iv <sup>d</sup> 10 mg/kg	oral <sup>d</sup> 10 mg/kg	oral <sup>d</sup> 100 mg/kg	
solubility pH 7 ( $\mu\text{M}$ )	194	$C_{\max}$ ( $\mu\text{M}$ )	5.6 $\pm$ 0.1	5.2 $\pm$ 0.6	6.0 $\pm$ 0.7	2.8 $\pm$ 0.3	17.7 $\pm$ 1.1
permeability PAMPA $P_{app}$ [ $10^{-6}\text{cm/s}$ ] (% in membrane)	29.1 (10.0)	AUC $_{0\infty}$ ( $\mu\text{M}\cdot\text{h}$ )	20.7 $\pm$ 2.3	19.7 $\pm$ 5.2	40.0 $\pm$ 8.0	34 $\pm$ 2.9	251.0 $\pm$ 30.5
PPB <sup>e</sup> (%)	78	CL (mL/min/kg)	19.3 $\pm$ 2.3		10.8 $\pm$ 2.4		
CL (mL/min/kg) HLM <sup>f</sup>	5	V <sub>ss</sub> (L/kg)	3.9 $\pm$ 0.1		3.5 $\pm$ 0.6		
CL (mL/min/kg) rat hepatocytes	5	$t_{1/2}$ (h)	3.3 $\pm$ 0.1	3.1 $\pm$ 0.1	4.7 $\pm$ 1.2	3.9 $\pm$ 0.1	nm <sup>g</sup>
		$F^h$ (%)	95			87	65

<sup>a</sup>Harlan Nu/Nu mice;  $n = 3$  animals per study. <sup>b</sup>Sprague–Dawley rat;  $n = 3$  animals per study. <sup>c</sup>Dosed iv (intravenous administration), 10% Tween 80 in 5% dextrose; dosed per os (oral administration), 0.5% methocel. <sup>d</sup>Dosed iv (intravenous administration), 20% DMSO + 40% PEG 400 in 5% dextrose; dosed per os (oral administration), 0.5% methocel. <sup>e</sup>Plasma protein binding. <sup>f</sup>Human liver microsomes. <sup>g</sup>nm: not measurable.

<sup>h</sup>Bioavailability.

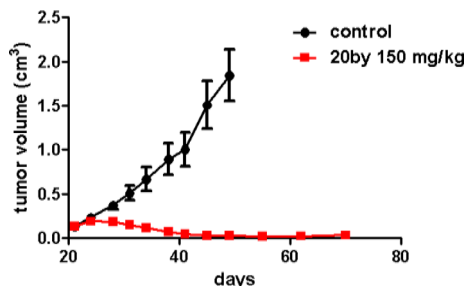


Figure 7. Antitumor efficacy of 20by in BRCA mutated breast cancer model in mice. Mice carrying subcutaneous MDA-MB-436 human breast carcinoma were treated with either vehicle or 20by orally administered. Mice were treated once a day for 28 days starting from day 20. Data are represented as mean  $\pm$  SEM.

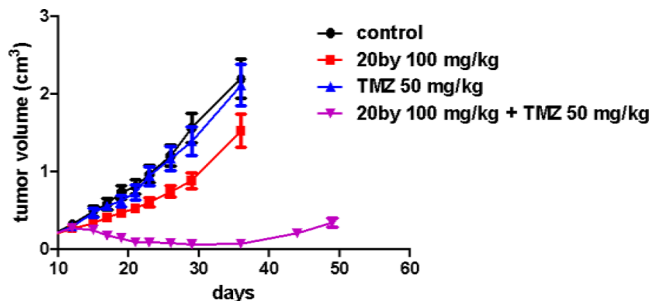


Figure 8. Antitumor efficacy of 20by in combination with Temozolomide. 20by was administered to male athymic nu/nu mice carrying subcutaneously Capan-1 pancreatic cancer, orally once daily for 12 days at the dose of 100 mg/kg, starting on day 9. Temozolomide (TMZ) was administered at a dosage of 50 mg/kg for 5 days starting from day 11. Data are represented as mean  $\pm$  SEM.

100 mg/kg of compound. Tumors were harvested at 1, 2, and 24 h after treatment, and intratumor PAR levels were determined by ELISA. 20by treatment dramatically decreased intratumoral PAR levels at 1, 2, and 6 h after administration, confirming its expected mechanism of action also *in vivo*. Partial recovery of PAR levels was observed at 24 h (Figure 9).

## CONCLUSION

PARP inhibitors currently undergoing clinical trials in oncology are unselective PARP-1/-2 inhibitors. Poly(ADP-ribose) polymerase-2 (PARP-2), the closest isoform of PARP-1, has a number of reported physiological functions other than its

subsidiary role in DNA repair. These considerations inspired our efforts toward developing selective PARP-1 inhibitors as potentially better tolerated drugs, especially in view of potential drug/drug combination settings. An HTS campaign on our proprietary collection was performed, followed by an intensive medicinal chemistry exploration around the resulting moderately potent, but unselective isoindolinone-4-carboxamide hits 10a and 10b. Investigation of the substituent on the nitrogen atom of the bicyclic core allowed the discovery of the selective 13af, whose cellular activity and pharmacokinetic properties were, however, still suboptimal. To further gain insight into the SAR of isoindolinone-4-carboxamides, a completely different synthetic route was then implemented to access derivatives modified on the aromatic ring of the bicyclic scaffold. These efforts successfully culminated in the discovery of 20by (NMS-P118), a potent and exceedingly selective PARP-1 inhibitor, whose unprecedented selectivity might reside in its distinct binding poses within the catalytic domains of PARP-1 and PARP-2. NMS-P118 shows excellent ADME and pharmacokinetic profiles, high oral availability in the mouse and rat, and high efficacy both as a single agent and in combination with Temozolomide in BRCA1-mutated MDA-MB-436 and BRCA2 deficient Capan-1 human tumor xenograft models, respectively. NMS-P118 was found to be less myelotoxic *in vitro* than olaparib (now marketed as Lynparza), a dual PARP-1/-2 inhibitor. NMS-P118 is, to our knowledge, the first PARP-1 selective inhibitor with demonstrated anticancer activity as single agent, as well as in combination, and thus we provide compelling proof-of-concept that the sole pharmacological inhibition of PARP-1 vs PARP-2 is sufficient for achieving high antitumor efficacy in BRCA deficient tumor settings.

## EXPERIMENTAL SECTION

**1. Chemistry.** All solvents and reagents, unless otherwise stated, were high grade, commercially available, and were used without further purification. All experiments dealing with moisture-sensitive compounds were conducted under dry nitrogen or argon. Organic solutions were evaporated using a Heidolph WB 2001 rotary evaporator at 15–20 mmHg. Thin-layer chromatography was performed on Merck silica gel 60 F<sub>254</sub> precoated plates. Flash chromatography was performed on silica gel (Merck grade 9395, 60A). All tested compounds, reported in the present paper, possess a purity of at least 95% as determined by an HPLC-UV/MS method. HPLC analyses were performed on Waters Xterra RP18 (4.6 mm  $\times$  50 mm, 3.5  $\mu\text{m}$ ) column using a Waters 2790 HPLC system equipped with a 996 Waters PDA detector and Micromass ZQ single quadrupole mass spectrometer, equipped with an

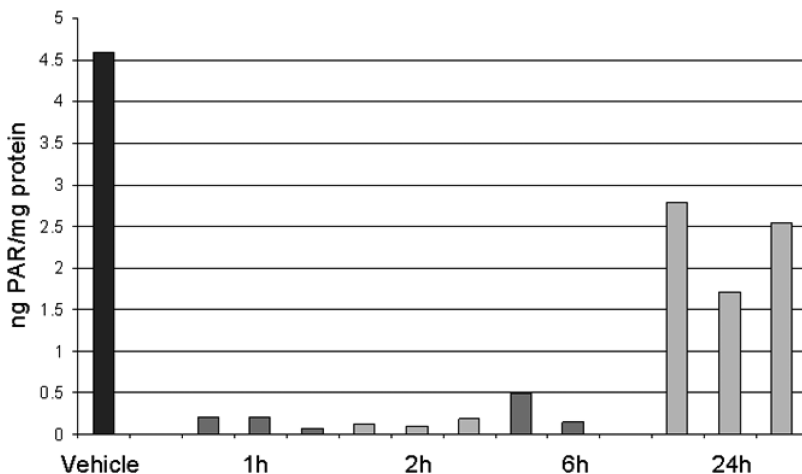


**Figure 9.** In vivo inhibition of PAR activity. Mice were treated with a single oral dose of **20by** (100 mg/kg), and intratumoral levels of PAR were assessed by ELISA at 1, 2, 6, and 24 h after dosing. Each bar represents an individual tumor from an individual animal.

electrospray (ESI) ion source. Mobile phase A was ammonium acetate 5 mM buffer (pH 5.5 with AcOH–acetonitrile 95:5), and mobile phase B was water–acetonitrile (5:95); gradient from 10 to 90% B in 8 min, hold 90% B 2 min; UV detection at 220 and 254 nm; flow rate 1 mL/min; injection volume 10  $\mu$ L. Full scan mass spectra were recorded in the mass range of 100–800 amu. Capillary voltage was 2.5 kV; source temperature was 120 °C; cone was 10 V. Masses are given as *m/z* ratio. When necessary, compounds were purified by preparative HPLC on a Waters Symmetry C18 (19 mm × 50 mm, 5  $\mu$ m) column or on a Waters XTerra RP 18 (30 mm × 150 mm, 5  $\mu$ m) column using a Waters preparative HPLC 600 equipped with a 996 Waters PDA detector and a Micromass ZMD single quadrupole mass spectrometer, electrospray ionization (positive ion mode). Mobile phase A was water–0.01% TFA, and mobile phase B was acetonitrile; gradient from 10 to 90% B in 8 min, hold 90% B 2 min; flow rate 20 mL/min. Alternatively, mobile phase A was water–0.1% NH<sub>4</sub>OH, and mobile phase B was acetonitrile; gradient from 10 to 100% B in 8 min, hold 100% B 2 min; flow rate 20 mL/min. <sup>1</sup>H NMR spectra were recorded at 28 °C on a Varian INOVA 400 spectrometer operating at 400.5 MHz for <sup>1</sup>H and equipped with 5 mm <sup>1</sup>H{<sup>15</sup>N, <sup>31</sup>P} z axis PFG indirect detection probe, at 25 °C on a Varian INOVA 500 spectrometer operating at 499.75 MHz for <sup>1</sup>H and equipped with 5 mm <sup>1</sup>H{<sup>13</sup>C, <sup>15</sup>N} z axis PFG indirect detection probe and on a Varian Mercury 300 spectrometer operating at 300.5 MHz for <sup>1</sup>H and equipped with 5 mm PFG autoswitchable <sup>1</sup>H, <sup>19</sup>F, <sup>13</sup>C, <sup>31</sup>P probe. Spectra were recorded in DMSO-*d*<sub>6</sub> or CDCl<sub>3</sub>. Chemical shifts were referenced with respect to the residual solvent signal (DMSO-*d*<sub>6</sub>, 2.50 ppm; CDCl<sub>3</sub>, 7.27 ppm). Data are reported as follows: chemical shift ( $\delta$ ), multiplicity (s = singlet, d = doublet, t = triplet, q = quartet, bs = broad signal, td = triplet of doublets, dd = doublet of doublets, ddd = doublet of triplets of doublets, m = multiplet), coupling constants (Hz), and number of protons. As formerly reported,<sup>44</sup> ESI(+) high-resolution mass spectra (HRMS) were obtained on a Q-ToF Ultima (Waters, Manchester, UK) mass spectrometer directly connected with an Agilent 1100 micro-HPLC system (Palo Alto, US).

**1-Benzyl-N-(furan-2-ylmethyl)piperidin-4-amine (7u).** An equimolar solution of furan-2-carbaldehyde (4.8 g, 50 mmol) and 1-benzylpiperidin-4-amine **6u** (9.5 g, 50 mmol) in dioxane (30 mL) was heated to reflux for 8 h by employing a Dean–Stark apparatus. The reaction mixture was concentrated under vacuum and rinsed with ethanol (1000 mL). Sodium borohydride (2.08 g, 55 mmol) was added, and the mixture was left overnight at room temperature. Then it was diluted with water and extracted with diethyl ether. The organic phase was dried over anhydrous sodium sulfate and concentrated under reduced pressure to give the title compound, employed in the following steps without any further purification.

**2-(1-Benzylpiperidin-4-yl)-1-oxo-1,2,3,6,7,7a-hexahydro-3a,6-epoxyisoindole-7-carboxylic Acid (8u).** To a solution of **7u** (13.3 g,

50 mmol) in tetrahydrofuran (140 mL), maleic anhydride (4.9 g, 50 mmol) was added. The reaction mixture was refluxed for 6 h and stirred overnight at room temperature. The precipitate solid obtained was filtered, washed with diethyl ether, and dried to give the desired compound as a white solid. ESI(+) MS: *m/z* 369 (MH<sup>+</sup>).

**2-(1-Benzylpiperidin-4-yl)-3-oxo-2,3-dihydro-1H-isoindole-4-carboxylic Acid (9u).** Compound **8u** (18.4 g, 50 mmol) was dissolved in 37% hydrochloric acid (150 mL), and the solution was refluxed for 3 h. The solvent was removed under reduced pressure to afford the resulting crude as hydrochloride salt. HRMS (ESI+): calcd for C<sub>21</sub>H<sub>23</sub>N<sub>2</sub>O<sub>3</sub><sup>+</sup> [M + H]<sup>+</sup> 351.1703; found 351.1706.

**2-(1-Benzylpiperidin-4-yl)-3-oxo-2,3-dihydro-1H-isoindole-4-carboxamide (10u).** To a solution of **9u** (19.3 g, 50 mmol) in *N,N*-dimethylformamide (300 mL) hydroxybenzotriazole ammonium salt (15.2 g, 100 mmol), 1-ethyl-3-(3'-dimethylamino)carbodiimide hydrochloric acid salt (19.2 g, 100 mmol) and triethylamine (17 mL, 200 mmol) were added. The reaction mixture was stirred at room temperature overnight. The solvent was removed under reduced pressure, and the residue was dissolved in ethyl acetate. The solution was washed with 15% ammonium hydroxide, and the organic phase was dried over anhydrous sodium sulfate and concentrated in vacuo. The crude was purified by flash chromatography (dichloromethane/methanol 97:3) to afford the title compound (3.5 g, 20% over four steps) as a white solid. <sup>1</sup>H NMR (400 MHz, DMSO-*d*<sub>6</sub>)  $\delta$  10.72 (bs, 1H), 8.20 (dd, *J* = 7.4, 1.5 Hz, 1H), 7.76 (dd, *J* = 7.4, 1.5 Hz, 1H), 7.71 (dd, *J* = 7.4, 7.4 Hz, 1H), 7.66 (bs, 1H), 7.36–7.30 (m, 4H), 7.30–7.20 (m, 1H), 4.56 (s, 2H), 4.11–4.00 (m, 1H), 3.51 (s, 2H), 2.96–2.88 (m, 2H), 2.15–2.03 (m, 2H), 1.90–1.70 (m, 4H). HRMS (ESI+): calcd for C<sub>21</sub>H<sub>24</sub>N<sub>3</sub>O<sub>2</sub><sup>+</sup> [M + H]<sup>+</sup> 350.1863; found 350.1874

**Compounds 10a–10t.** By employment of the above-described procedure and using the suitably substituted amine **6a–t**, compounds **10a–t** were obtained.

**3-Oxo-2-propyl-2,3-dihydro-1H-isoindole-4-carboxamide (10a).** <sup>1</sup>H NMR (400 MHz, DMSO-*d*<sub>6</sub>)  $\delta$  10.76 (bs, 1H), 8.20 (d, *J* = 7.6 Hz, 1H), 7.76 (d, *J* = 7.3 Hz, 1H), 7.72 (dd, *J* = 7.6, 7.3 Hz, 1H), 7.66 (bs, 1H), 4.57 (s, 2H), 3.56–3.51 (m, 2H), 1.71–1.61 (m, 2H), 0.89 (t, *J* = 7.3 Hz, 3H). HRMS (ESI+): calcd for C<sub>12</sub>H<sub>15</sub>N<sub>2</sub>O<sub>2</sub><sup>+</sup> [M + H]<sup>+</sup> 219.1128; found 219.1122.

**2-(3-Methoxypropyl)-3-oxo-2,3-dihydro-1H-isoindole-4-carboxamide (10b).** <sup>1</sup>H NMR (400 MHz, DMSO-*d*<sub>6</sub>)  $\delta$  10.75 (bs, 1H), 8.21 (d, *J* = 7.7 Hz, 1H), 7.77 (d, *J* = 7.3 Hz, 1H), 7.72 (dd, *J* = 7.7, 7.3 Hz, 1H), 7.67 (bs, 1H), 4.58 (s, 2H), 3.66–3.60 (m, 2H), 3.40–3.36 (m, 2H), 3.24 (s, 3H), 1.92–1.84 (m, 2H). HRMS (ESI+): calcd for C<sub>13</sub>H<sub>17</sub>N<sub>2</sub>O<sub>3</sub><sup>+</sup> [M + H]<sup>+</sup> 249.1234; found 249.1232.

**2-(2-Methoxyethyl)-3-oxo-2,3-dihydro-1H-isoindole-4-carboxamide (10c).** <sup>1</sup>H NMR (400 MHz, DMSO-*d*<sub>6</sub>)  $\delta$  10.68 (bs, 1H), 8.20 (dd, *J* = 7.5, 1.3 Hz, 1H), 7.77 (dd, *J* = 7.6, 1.3 Hz, 1H), 7.72 (dd, *J* = 7.6, 7.5 Hz, 1H), 7.67 (bs, 1H), 4.61 (s, 2H), 3.75 (t, *J* = 5.3 Hz, 2H),

3.60 (t,  $J = 5.3$  Hz, 2H), 3.28 (s, 3H). HRMS (ESI+): calcd for  $C_{12}H_{13}N_2O_3^+ [M + H]^+$  235.1077; found 235.1083.

**3-Oxo-2-(tetrahydrofuran-2-ylmethyl)-2,3-dihydro-1H-isoindole-4-carboxamide ( $\pm$ -10d).**  $^1$ H NMR (400 MHz, DMSO- $d_6$ )  $\delta$  10.66 (bs, 1H), 8.20 (dd,  $J = 7.5, 1.3$  Hz, 1H), 7.77 (dd,  $J = 7.6, 1.3$  Hz, 1H), 7.72 (dd,  $J = 7.6, 7.5$  Hz, 1H), 7.67 (bs, 1H), 4.71–4.58 (m, 2H), 4.14–4.07 (m, 1H), 3.84–3.76 (m, 1H), 3.73–3.55 (m, 3H), 1.93–2.02 (m, 1H), 1.88–1.77 (m, 2H), 1.63–1.53 (m, 1H). HRMS (ESI+): calcd for  $C_{14}H_{17}N_2O_3^+ [M + H]^+$  261.1234; found 261.1242.

**2-(2-Hydroxyethyl)-3-oxo-2,3-dihydro-1H-isoindole-4-carboxamide (10e).**  $^1$ H NMR (400 MHz, DMSO- $d_6$ )  $\delta$  10.77 (bs, 1H), 8.21 (dd,  $J = 7.4, 1.2$  Hz, 1H), 7.77 (dd,  $J = 7.6, 1.2$  Hz, 1H), 7.72 (dd,  $J = 7.6, 7.4$  Hz, 1H), 7.66 (bs, 1H), 4.87 (t,  $J = 5.2$  Hz, 1H), 4.63 (s, 2H), 3.70–3.60 (m, 4H). HRMS (ESI+): calcd for  $C_{11}H_{13}N_2O_3^+ [M + H]^+$  221.0921; found 221.0919.

**2-Benzyl-3-oxo-2,3-dihydro-1H-isoindole-4-carboxamide (10f).**  $^1$ H NMR (400 MHz, DMSO- $d_6$ )  $\delta$  10.59 (bs, 1H), 8.22–8.17 (m, 1H), 7.75–7.69 (m, 3H), 7.40–7.28 (m, 5H), 4.79 (s, 2H), 4.47 (s, 2H). HRMS (ESI+): calcd for  $C_{16}H_{15}N_2O_2^+ [M + H]^+$  267.1128; found 267.1120.

**3-Oxo-2-(2-phenylethyl)-2,3-dihydro-1H-isoindole-4-carboxamide (10g).**  $^1$ H NMR (400 MHz, DMSO- $d_6$ )  $\delta$  10.68 (bs, 1H), 8.19 (dd,  $J = 7.3, 1.6$  Hz, 1H), 7.74 (dd,  $J = 7.6, 1.6$  Hz, 1H), 7.70 (dd,  $J = 7.6, 7.3$  Hz, 1H), 7.66 (bs, 1H), 7.32–7.25 (m, 4H), 7.23–7.18 (m, 1H), 4.49 (s, 2H), 3.85–3.80 (m, 2H), 3.00–2.94 (m, 2H). HRMS (ESI+): calcd for  $C_{17}H_{17}N_2O_2^+ [M + H]^+$  281.1285; found 281.1295.

**3-Oxo-2-(3-phenylpropyl)-2,3-dihydro-1H-isoindole-4-carboxamide (10h).**  $^1$ H NMR (400 MHz, DMSO- $d_6$ )  $\delta$  10.74 (bs, 1H), 8.21 (dd,  $J = 7.4, 1.5$  Hz, 1H), 7.78–7.75 (m, 1H), 7.75–7.70 (m, 1H), 7.67 (bs, 1H), 7.31–7.24 (m, 4H), 7.20–7.15 (m, 1H), 4.59 (s, 2H), 3.64–3.59 (m, 2H), 2.67–2.60 (m, 2H), 2.01–1.92 (m, 2H). HRMS (ESI+): calcd for  $C_{18}H_{19}N_2O_2^+ [M + H]^+$  295.1441; found 295.1433.

**3-Oxo-2-[2-(pyridin-2-yl)ethyl]-2,3-dihydro-1H-isoindole-4-carboxamide (10i).**  $^1$ H NMR (400 MHz, DMSO- $d_6$ )  $\delta$  10.66 (bs, 1H), 8.48 (ddd,  $J = 4.9, 1.8, 1.0$  Hz, 1H), 8.19 (dd,  $J = 7.4, 1.5$  Hz, 1H), 7.75 (dd,  $J = 7.6, 1.5$  Hz, 1H), 7.73–7.68 (m, 2H), 7.65 (bs, 1H), 7.32 (td,  $J = 7.8, 1.0$  Hz, 1H), 7.23 (ddd,  $J = 7.5, 4.9, 1.0$  Hz, 1H), 4.52 (s, 2H), 3.98–3.93 (m, 2H), 3.15–3.10 (m, 2H). HRMS (ESI+): calcd for  $C_{16}H_{16}N_3O_2^+ [M + H]^+$  282.1237; found 282.1243.

**2-[2-(Morpholin-4-yl)ethyl]-3-oxo-2,3-dihydro-1H-isoindole-4-carboxamide (10j).**  $^1$ H NMR (400 MHz, DMSO- $d_6$ )  $\delta$  10.73 (bs, 1H), 8.20 (dd,  $J = 7.5, 1.3$  Hz, 1H), 7.78 (dd,  $J = 7.6, 1.3$  Hz, 1H), 7.72 (dd,  $J = 7.6, 7.5$  Hz, 1H), 7.66 (bs, 1H), 4.64 (s, 2H), 3.71 (t,  $J = 6.2$  Hz, 2H), 3.57–3.52 (m, 4H), 2.59 (t,  $J = 6.2$  Hz, 2H), 2.46–2.41 (m, 4H). HRMS (ESI+): calcd for  $C_{15}H_{20}N_3O_3^+ [M + H]^+$  290.1499; found 290.1507.

**2-[3-(Morpholin-4-yl)propyl]-3-oxo-2,3-dihydro-1H-isoindole-4-carboxamide (10k).**  $^1$ H NMR (400 MHz, DMSO- $d_6$ )  $\delta$  10.76 (bs, 1H), 8.20 (dd,  $J = 7.5, 1.2$  Hz, 1H), 7.76 (dd,  $J = 7.6, 1.2$  Hz, 1H), 7.71 (dd,  $J = 7.6, 7.5$  Hz, 1H), 7.65 (bs, 1H), 4.58 (s, 2H), 3.61 (t,  $J = 7.1$  Hz, 2H), 3.53–3.47 (m, 4H), 2.37–2.29 (m, 6H), 1.85–1.76 (m, 2H). HRMS (ESI+): calcd for  $C_{16}H_{22}N_3O_2^+ [M + H]^+$  304.1656; found 304.1664.

**3-Oxo-2-[2-(piperidin-1-yl)ethyl]-2,3-dihydro-1H-isoindole-4-carboxamide (10l).**  $^1$ H NMR (400 MHz, DMSO- $d_6$ )  $\delta$  10.75 (bs, 1H), 8.20 (dd,  $J = 7.7, 1.2$  Hz, 1H), 7.78 (dd,  $J = 7.4, 1.2$  Hz, 1H), 7.72 (dd,  $J = 7.7, 7.4$  Hz, 1H), 7.66 (bs, 1H), 4.63 (s, 2H), 3.68 (t,  $J = 6.3$  Hz, 2H), 2.54 (t,  $J = 6.3$  Hz, 2H), 2.43–2.36 (m, 4H), 1.50–1.42 (m, 4H), 1.41–1.32 (m, 2H). HRMS (ESI+): calcd for  $C_{16}H_{22}N_3O_2^+ [M + H]^+$  288.1707; found 288.1712.

**3-Oxo-2-[3-(piperidin-1-yl)propyl]-2,3-dihydro-1H-isoindole-4-carboxamide Hydrochloride (10m).**  $^1$ H NMR (400 MHz, DMSO- $d_6$ )  $\delta$  10.58 (bs, 1H), 8.93 (bs, 1H), 8.21 (dd,  $J = 7.6, 1.1$  Hz, 1H), 7.80 (dd,  $J = 7.4, 1.1$  Hz, 1H), 7.74 (dd,  $J = 7.6, 7.4$  Hz, 1H), 7.71 (bs, 1H), 4.59 (s, 2H), 3.66 (t,  $J = 6.6$  Hz, 2H), 3.50–3.40 (m, 2H), 3.13–3.03 (m, 2H), 2.92–2.78 (m, 2H), 2.09–1.98 (m, 2H), 1.85–1.75 (m, 2H), 1.73–1.52 (m, 3H), 1.43–1.28 (m, 1H). HRMS (ESI+): calcd for  $C_{17}H_{24}N_3O_2^+ [M + H]^+$  302.1863; found 302.1865.

**cis-2-[3-(2,6-Dimethylpiperidin-1-yl)propyl]-3-oxo-2,3-dihydro-1H-isoindole-4-carboxamide (cis-10n).**  $^1$ H NMR (400 MHz, DMSO- $d_6$ )  $\delta$  10.58 (bs, 1H), 8.72 (bs, 1H), 8.21 (dd,  $J = 7.5, 1.2$  Hz, 1H),

7.80 (dd,  $J = 7.6, 1.2$  Hz, 1H), 7.74 (dd,  $J = 7.6, 7.5$  Hz, 1H), 7.70 (bs, 1H), 4.63 (s, 2H), 3.72–3.64 (m, 2H), 3.35–3.20 (m partially overlapped by water signal, 4H), 2.06–1.93 (m, 2H), 1.89–1.80 (m, 2H), 1.54–1.43 (m, 4H), 1.25 (d,  $J = 6.3$  Hz, 6H). HRMS (ESI+): calcd for  $C_{19}H_{28}N_3O_2^+ [M + H]^+$  330.2176; found 330.2176.

**2-[3-(1*A*,4'-Bipiperidin-1'-yl)propyl]-3-oxo-2,3-dihydro-1H-isoindole-4-carboxamide Dihydrochloride (10o).**  $^1$ H NMR (400 MHz, DMSO- $d_6$ )  $\delta$  10.58 (bs, 1H), 9.38 (bs, 2H), 8.21 (dd,  $J = 7.6, 1.2$  Hz, 1H), 7.80 (d,  $J = 7.5, 1$  H), 7.75 (dd,  $J = 7.6, 7.5$  Hz, 1H), 7.72 (bs, 1H), 4.59 (s, 2H), 3.70–2.82 (m, 13H), 2.30–1.30 (m, 12H). HRMS (ESI+): calcd for  $C_{22}H_{33}N_4O_2^+ [M + H]^+$  385.2598; found 385.2611.

**2-[3-(4-Benzylpiperidin-1-yl)propyl]-3-oxo-2,3-dihydro-1H-isoindole-4-carboxamide (10p).**  $^1$ H NMR (400 MHz, DMSO- $d_6$ )  $\delta$  10.78 (bs, 1H), 8.21 (dd,  $J = 7.4, 1.3$  Hz, 1H), 7.76 (dd,  $J = 7.5, 1.3$  Hz, 1H), 7.72 (dd,  $J = 7.5, 7.4$  Hz, 1H), 7.65 (bs, 1H), 7.28–7.23 (m, 2H), 7.19–7.13 (m, 1H), 7.12–7.09 (m, 2H), 4.56 (s, 2H), 3.62–3.56 (m, 2H), 2.87–2.74 (m, 2H), 2.41 (d,  $J = 6.8$  Hz, 2H), 2.33–2.22 (m, 2H), 1.82–1.70 (m, 4H), 1.52–1.37 (m, 3H), 1.11–0.99 (m, 2H). HRMS (ESI+): calcd for  $C_{24}H_{30}N_3O_2^+ [M + H]^+$  392.2333; found 392.2346.

**2-[2-(3,4-Dihydroquinolin-1(2H)-yl)ethyl]-3-oxo-2,3-dihydro-1H-isoindole-4-carboxamide (10q).**  $^1$ H NMR (400 MHz, DMSO- $d_6$ )  $\delta$  10.68 (bs, 1H), 8.20 (dd,  $J = 7.6, 1.3$  Hz, 1H), 7.77 (dd,  $J = 7.4, 1.3$  Hz, 1H), 7.72 (dd,  $J = 7.6, 7.4$  Hz, 1H), 7.69 (bs, 1H), 6.97–6.92 (m, 1H), 6.88–6.85 (m, 1H), 6.75–6.70 (m, 1H), 6.49–6.44 (m, 1H), 4.65 (s, 2H), 3.78–3.73 (m, 2H), 3.58–3.53 (m, 2H), 3.34–3.28 (m overlapped by water signal, 2H), 2.69–2.65 (m, 2H), 1.88–1.80 (m, 2H). HRMS (ESI+): calcd for  $C_{20}H_{22}N_3O_2^+ [M + H]^+$  336.1707; found 336.1692.

**2-[2-(3,4-Dihydroisoquinolin-2(1H)-yl)ethyl]-3-oxo-2,3-dihydro-1H-isoindole-4-carboxamide (10r).**  $^1$ H NMR (400 MHz, DMSO- $d_6$ )  $\delta$  10.75 (bs, 1H), 8.19 (dd,  $J = 7.6, 1.2$  Hz, 1H), 7.76 (dd,  $J = 7.7, 1.2$  Hz, 1H), 7.69 (dd,  $J = 7.7, 7.6$  Hz, 1H), 7.66 (bs, 1H), 7.11–7.00 (m, 4H), 4.65 (s, 2H), 3.81 (t,  $J = 6.2$  Hz, 2H), 3.65 (s, 2H), 2.82–2.73 (bs, 6H). HRMS (ESI+): calcd for  $C_{20}H_{22}N_3O_2^+ [M + H]^+$  336.1707; found 336.1722.

**2-[{[1-(4-Methylbenzyl)piperidin-4-yl]methyl}-3-oxo-2,3-dihydro-1H-isoindole-4-carboxamide (10s).**  $^1$ H NMR (400 MHz, DMSO- $d_6$ )  $\delta$  10.72 (bs, 1H), 8.20 (dd,  $J = 7.4, 1.6$  Hz, 1H), 7.77–7.74 (m, 1H), 7.74–7.69 (m, 1H), 7.66 (bs, 1H), 7.20–7.07 (m, 4H), 4.57 (s, 2H), 3.46 (d,  $J = 7.2$  Hz, 2H), 3.39 (s, 2H), 2.82–2.72 (m, 2H), 2.27 (s, 3H), 1.95–1.82 (m, 2H), 1.82–1.68 (m, 1H), 1.65–1.53 (m, 2H), 1.30–1.16 (m, 2H). HRMS (ESI+): calcd for  $C_{23}H_{28}N_3O_2^+ [M + H]^+$  378.2176; found 378.2183.

**2-[{[1-(3-Methylbenzyl)piperidin-4-yl]methyl}-3-oxo-2,3-dihydro-1H-isoindole-4-carboxamide (10t).**  $^1$ H NMR (400 MHz, DMSO- $d_6$ )  $\delta$  10.72 (bs, 1H), 8.20 (dd,  $J = 7.3, 1.5$  Hz, 1H), 7.77–7.73 (m, 1H), 7.73–7.69 (m, 1H), 7.66 (bs, 1H), 7.20–7.15 (m, 1H), 7.11–7.00 (m, 3H), 4.57 (s, 2H), 3.46 (d,  $J = 7.3$  Hz, 2H), 3.39 (s, 2H), 2.80–2.74 (m, 2H), 2.28 (s, 3H), 1.94–1.85 (m, 2H), 1.83–1.70 (m, 1H), 1.62–1.54 (m, 2H), 1.29–1.18 (m, 2H). HRMS (ESI+): calcd for  $C_{23}H_{28}N_3O_2^+ [M + H]^+$  378.2176; found 378.2188.

**3-Oxo-2-(piperidin-4-yl)-2,3-dihydro-1H-isoindole-4-carboxamide Hydrochloride (11).** A solution of **10u** (1.3 g, 3.72 mmol) in acetic acid (100 mL) in the presence of Pd/C 10% (260 mg) was hydrogenated at 50 psi for 8 h. The mixture was filtered over a pad of Celite, and the solution was concentrated to afford the title compound (900 mg, 93%).  $^1$ H NMR (400 MHz, DMSO- $d_6$ )  $\delta$  10.58 (bs, 1H), 8.82 (bs, 1H), 8.59 (bs, 1H), 8.21 (dd,  $J = 7.5, 1.1$  Hz, 1H), 7.82 (dd,  $J = 7.6, 1.1$  Hz, 1H), 7.75 (dd,  $J = 7.6, 7.5$  Hz, 1H), 7.71 (bs, 1H), 4.56 (s, 2H), 4.32–4.45 (m, 1H), 3.46–3.36 (m overlapped by water signal, 2H), 3.17–3.04 (m, 2H), 2.09–1.92 (m, 4H). HRMS (ESI+): calcd for  $C_{14}H_{18}N_3O_2^+ [M + H]^+$  260.1394; found 260.1398.

**2-[{[1-(Cyclopropylcarbonyl)piperidin-4-yl]methyl}-3-oxo-2,3-dihydro-1H-isoindole-4-carboxamide (12b).** To a solution of **11** (60 mg, 0.23 mmol) in pyridine (2 mL) cyclopropanecarbonyl chloride (26.4 mg, 0.25 mmol) was added. After stirring at 60 °C for 8 h, the solvent was removed under reduced pressure and the crude was purified by flash chromatography (dichloromethane/methanol 95:5) to give the desired compound (32 mg, 40%).  $^1$ H NMR (400 MHz, DMSO- $d_6$ )  $\delta$  10.70 (bs, 1H), 8.21 (dd,  $J = 7.2, 1.6$  Hz, 1H), 7.78–7.75

(m, 1H), 7.75–7.71 (m, 1H), 7.69 (bs, 1H), 4.57 (s, 2H), 4.60–4.38 (m, 2H), 4.40–4.30 (m, 1H), 3.40–3.19 (m partially overlapped by water signal, 1H), 2.76–2.65 (m, 1H), 2.07–2.00 (m, 1H), 1.97–1.54 (m, 4H), 0.83–0.67 (m, 4H). HRMS (ESI+): calcd for  $C_{18}H_{22}N_3O_3^+$  [M + H]<sup>+</sup> 328.1656; found 328.1669.

**Compounds 12a–12c.** Operating in an analogous way but employing suitably substituted starting material, the following compounds were obtained:

**2-(1-Acetyl <sup>1</sup>H NMR (400 MHz, DMSO-*d*<sub>6</sub>)  $\delta$  10.69 (bs, 1H), 8.21 (dd, *J* = 7.3, 1.5 Hz, 1H), 7.78–7.75 (m, 1H), 7.75–7.70 (m, 1H), 7.69 (bs, 1H), 4.55 (s, 2H), 4.58–4.49 (m, 1H), 4.36–4.26 (m, 1H), 3.99–3.91 (m, 1H), 3.15–3.25 (m, 1H), 2.70–2.60 (m, 1H), 2.04 (s, 3H), 1.90–1.70 (m, 3H), 1.68–1.55 (m, 1H). HRMS (ESI+): calcd for  $C_{16}H_{20}N_3O_3^+$  [M + H]<sup>+</sup> 302.1499; found 302.1506.**

**2-[1-(Cyclohexylcarbonyl)piperidin-4-yl]-3-oxo-2,3-dihydro-1H-isoindole-4-carboxamide (12c).** <sup>1</sup>H NMR (400 MHz, DMSO-*d*<sub>6</sub>)  $\delta$  10.69 (bs, 1H), 8.21 (dd, *J* = 7.2, 1.7 Hz, 1H), 7.77–7.70 (m, 2H), 7.69 (bs, 1H), 4.62–4.50 (m, 1H), 4.56 (s, 2H), 4.37–4.27 (m, 1H), 4.13–4.02 (m, 1H), 3.24–3.10 (m, 1H), 2.71–2.57 (m, 2H), 1.93–1.50 (m, 8H), 1.47–1.09 (m, 6H). HRMS (ESI+): calcd for  $C_{21}H_{28}N_3O_3^+$  [M + H]<sup>+</sup> 370.2125; found 370.2117.

**2-[1-(4,4-Difluorocyclohexyl)piperidin-4-yl]-3-oxo-2,3-dihydro-1H-isoindole-4-carboxamide (13af).** To a suspension of 11 (56 mg, 0.19 mmol) in dichloromethane (2 mL), 4,4-difluorocyclohexanone (37.5 mg, 0.28 mmol), sodium acetate (32 mg, 0.38 mmol), and methanol (0.3 mL) were added. The resulting solution was stirred at room temperature for 5 h. Then sodium cyanoborohydride was added and the mixture was stirred overnight. Solvents were removed under reduced pressure, and the residue was dissolved in dichloromethane and washed twice with water. The organic phase was dried over anhydrous sodium sulfate and concentrated in vacuo, and the residue was purified by flash chromatography (dichloromethane/methanol 95:5) to give the title compound (33 mg, 45%). <sup>1</sup>H NMR (400 MHz, DMSO-*d*<sub>6</sub>)  $\delta$  10.73 (bs, 1H), 8.20 (dd, *J* = 7.4, 1.5 Hz, 1H), 7.77–7.74 (m, 1H), 7.74–7.69 (m, 1H), 7.66 (bs, 1H), 4.55 (s, 2H), 4.09–3.95 (m, 1H), 3.00–2.90 (m, 2H), 2.66–2.44 (m overlapped by DMSO signal, 1H), 2.35–2.23 (m, 2H), 2.10–1.96 (m, 2H), 1.94–1.70 (m, 8H), 1.61–1.47 (m, 2H). HRMS (ESI+): calcd for  $C_{20}H_{26}F_2N_3O_2^+$  [M + H]<sup>+</sup> 378.1988; found 378.1982.

**Compounds 13a–13ag.** Operating in an analogous way but employing suitably substituted starting material, the following compounds were obtained:

**2-(1-Methyl <sup>1</sup>H NMR (400 MHz, DMSO-*d*<sub>6</sub>)  $\delta$  10.73 (bs, 1H), 8.21 (dd, *J* = 7.5, 1.2 Hz, 1H), 7.77 (dd, *J* = 7.6, 1.2 Hz, 1H), 7.73 (dd, *J* = 7.6, 7.5 Hz, 1H), 7.67 (bs, 1H), 4.56 (s, 2H), 4.06–3.98 (m, 1H), 2.91–2.85 (m, 2H), 2.21 (s, 3H), 2.06–1.97 (m, 2H), 1.88–1.78 (m, 2H), 1.78–1.70 (m, 2H). HRMS (ESI+): calcd for  $C_{15}H_{20}N_3O_2^+$  [M + H]<sup>+</sup> 274.1550; found 274.1557.**

**2-(1-Ethyl <sup>1</sup>H NMR (400 MHz, DMSO-*d*<sub>6</sub>)  $\delta$  10.73 (bs, 1H), 8.20 (dd, *J* = 7.5, 1.5 Hz, 1H), 7.77 (dd, *J* = 7.6, 1.5 Hz, 1H), 7.72 (dd, *J* = 7.6, 7.5 Hz, 1H), 7.66 (bs, 1H), 4.55 (s, 2H), 4.09–3.98 (m, 1H), 3.01–2.95 (m, 2H), 2.36 (*q*, *J* = 7.1 Hz, 2H), 2.02–1.95 (m, 2H), 1.85–1.72 (m, 4H), 1.01 (*t*, *J* = 7.1 Hz, 3H). HRMS (ESI+): calcd for  $C_{16}H_{22}N_3O_2^+$  [M + H]<sup>+</sup> 288.1707; found 288.1707.**

**3-Oxo-2-[1-(propan-2-yl)piperidin-4-yl]-2,3-dihydro-1H-isoindole-4-carboxamide (13c).** <sup>1</sup>H NMR (400 MHz, DMSO-*d*<sub>6</sub>)  $\delta$  10.74 (bs, 1H), 8.21 (dd, *J* = 7.5, 1.3 Hz, 1H), 7.77 (dd, *J* = 7.6, 1.3 Hz, 1H), 7.72 (dd, *J* = 7.6, 7.5 Hz, 1H), 7.67 (bs, 1H), 4.56 (s, 2H), 4.10–3.96 (m, 1H), 2.96–2.84 (m, 2H), 2.80–2.68 (m, 1H), 2.30–2.18 (m, 2H), 1.83–1.69 (m, 4H), 0.99 (*d*, *J* = 6.1 Hz, 6H). HRMS (ESI+): calcd for  $C_{17}H_{24}N_3O_2^+$  [M + H]<sup>+</sup> 302.1863; found 302.1862.

**2-[1-(2-Methylpropyl)piperidin-4-yl]-3-oxo-2,3-dihydro-1H-isoindole-4-carboxamide (13d).** <sup>1</sup>H NMR (400 MHz, DMSO-*d*<sub>6</sub>)  $\delta$  10.73 (bs, 1H), 8.20 (dd, *J* = 7.4, 1.5 Hz, 1H), 7.76 (*d*, *J* = 7.5 Hz, 1H), 7.72 (dd, *J* = 7.5, 7.4 Hz, 1H), 7.66 (bs, 1H), 4.56 (s, 2H), 4.08–3.98 (m, 1H), 2.96–2.89 (m, 2H), 2.06 (*d*, *J* = 6.2 Hz, 2H), 2.04–1.95 (m,

2H), 1.87–1.70 (m, 5H), 0.87 (d, *J* = 6.6 Hz, 6H). HRMS (ESI+): calcd for  $C_{18}H_{26}N_3O_2^+$  [M + H]<sup>+</sup> 316.2020; found 316.2020.

**2-[1-(Cyclopropylmethyl)piperidin-4-yl]-3-oxo-2,3-dihydro-1H-isoindole-4-carboxamide (13e).** <sup>1</sup>H NMR (400 MHz, DMSO-*d*<sub>6</sub>)  $\delta$  10.73 (bs, 1H), 8.20 (dd, *J* = 7.5, 1.2 Hz, 1H), 7.77 (dd, *J* = 7.6, 1.2 Hz, 1H), 7.72 (dd, *J* = 7.6, 7.5 Hz, 1H), 7.66 (bs, 1H), 4.56 (s, 2H), 4.10–3.97 (m, 1H), 3.13–3.04 (m, 2H), 2.21 (d, *J* = 6.3 Hz, 2H), 2.10–2.00 (m, 2H), 1.90–1.71 (m, 4H), 0.90–0.80 (m, 1H), 0.50–0.44 (m, 2H), 0.12–0.06 (m, 2H). HRMS (ESI+): calcd for  $C_{18}H_{24}N_3O_2^+$  [M + H]<sup>+</sup> 314.1863; found 314.1860.

**2-[1-(2-Methoxyethyl)piperidin-4-yl]-3-oxo-2,3-dihydro-1H-isoindole-4-carboxamide (13f).** <sup>1</sup>H NMR (400 MHz, DMSO-*d*<sub>6</sub>)  $\delta$  10.73 (bs, 1H), 8.20 (dd, *J* = 7.6, 1.3 Hz, 1H), 7.76 (dd, *J* = 7.4, 1.3 Hz, 1H), 7.71 (dd, *J* = 7.6, 7.4 Hz, 1H), 7.66 (bs, 1H), 4.55 (s, 2H), 4.08–3.97 (m, 1H), 3.44 (*t*, *J* = 5.8 Hz, 2H), 3.24 (s, 3H), 3.02–2.95 (m, 2H), 2.53–2.47 (m overlapped by DMSO signal, 2H), 2.14–2.06 (m, 2), 1.86–1.69 (m, 4H). HRMS (ESI+): calcd for  $C_{17}H_{24}N_3O_2^+$  [M + H]<sup>+</sup> 318.1812; found 318.1811.

**2-[1-(2-Methylbenzyl)piperidin-4-yl]-3-oxo-2,3-dihydro-1H-isoindole-4-carboxamide (13g).** <sup>1</sup>H NMR (400 MHz, DMSO-*d*<sub>6</sub>)  $\delta$  10.73 (bs, 1H), 8.20 (dd, *J* = 7.3, 1.6 Hz, 1H), 7.78–7.75 (m, 1H), 7.75–7.70 (m, 1H), 7.67 (bs, 1H), 7.28–7.23 (m, 1H), 7.19–7.12 (m, 3H), 4.57 (s, 2H), 4.14–4.02 (m, 1H), 3.47 (s, 2H), 2.96–2.88 (m, 2H), 2.35 (s, 3H), 2.19–2.10 (m, 2H), 1.88–1.73 (m, 4H). HRMS (ESI+): calcd for  $C_{22}H_{26}N_3O_2^+$  [M + H]<sup>+</sup> 364.2020; found 364.2034.

**2-[1-(3-Methylbenzyl)piperidin-4-yl]-3-oxo-2,3-dihydro-1H-isoindole-4-carboxamide (13h).** <sup>1</sup>H NMR (400 MHz, DMSO-*d*<sub>6</sub>)  $\delta$  10.73 (bs, 1H), 8.21 (dd, *J* = 7.3, 1.4 Hz, 1H), 7.77 (dd, *J* = 7.4, 1.4 Hz, 1H), 7.72 (dd, *J* = 7.4, 7.3 Hz, 1H), 7.67 (bs, 1H), 7.25–7.19 (m, 1H), 7.16–7.05 (m, 3H), 4.58 (s, 2H), 4.13–4.00 (m, 1H), 3.47 (s, 2H), 2.98–2.87 (m, 2H), 2.32 (s, 3H), 2.13–2.04 (m, 2H), 1.90–1.72 (m, 4H). HRMS (ESI+): calcd for  $C_{22}H_{26}N_3O_2^+$  [M + H]<sup>+</sup> 364.2020; found 364.2031.

**2-[1-(4-Methylbenzyl)piperidin-4-yl]-3-oxo-2,3-dihydro-1H-isoindole-4-carboxamide (13i).** <sup>1</sup>H NMR (400 MHz, DMSO-*d*<sub>6</sub>)  $\delta$  10.73 (bs, 1H), 8.20 (dd, *J* = 7.3, 1.5 Hz, 1H), 7.77 (dd, *J* = 7.4, 1.5 Hz, 1H), 7.72 (dd, *J* = 7.4, 7.3 Hz, 1H), 7.67 (bs, 1H), 7.23–7.18 (m, 2H), 7.16–7.12 (m, 2H), 4.57 (s, 2H), 4.11–4.00 (m, 1H), 3.46 (s, 2H), 2.96–2.88 (m, 2H), 2.30 (s, 3H), 2.12–2.03 (m, 2H), 1.88–1.71 (m, 4H). HRMS (ESI+): calcd for  $C_{22}H_{26}N_3O_2^+$  [M + H]<sup>+</sup> 364.2020; found 364.2033.

**2-[1-(2-Bromobenzyl)piperidin-4-yl]-3-oxo-2,3-dihydro-1H-isoindole-4-carboxamide (13j).** <sup>1</sup>H NMR (400 MHz, DMSO-*d*<sub>6</sub>)  $\delta$  10.73 (bs, 1H), 8.21 (dd, *J* = 7.3, 1.5 Hz, 1H), 7.77 (dd, *J* = 7.4, 1.5 Hz, 1H), 7.73 (dd, *J* = 7.4, 7.3 Hz, 1H), 7.68 (bs, 1H), 7.62 (dd, *J* = 7.9, 1.0 Hz, 1H), 7.52 (dd, *J* = 7.7, 1.3 Hz, 1H), 7.40 (td, *J* = 7.5, 1.0 Hz, 1H), 7.23 (td, *J* = 7.5, 1.3 Hz, 1H), 4.58 (s, 2H), 4.15–4.05 (m, 1H), 3.60 (s, 2H), 3.00–2.92 (m, 2H), 2.29–2.19 (m, 2H), 1.91–1.75 (m, 4H). HRMS (ESI+): calcd for  $C_{21}H_{23}BrN_3O_2^+$  [M + H]<sup>+</sup> 428.0968; found 428.0974.

**2-[1-(3-Bromobenzyl)piperidin-4-yl]-3-oxo-2,3-dihydro-1H-isoindole-4-carboxamide (13k).** <sup>1</sup>H NMR (400 MHz, DMSO-*d*<sub>6</sub>)  $\delta$  10.72 (bs, 1H), 8.21 (dd, *J* = 7.3, 1.5 Hz, 1H), 7.77 (dd, *J* = 7.4, 1.5 Hz, 1H), 7.73 (dd, *J* = 7.4, 7.3 Hz, 1H), 7.67 (bs, 1H), 7.54 (s, 1H), 7.49–7.45 (m, 1H), 7.37–7.30 (m, 2H), 4.58 (s, 2H), 4.12–4.00 (m, 1H), 3.53 (s, 2H), 2.95–2.88 (m, 2H), 2.17–2.08 (m, 2H), 1.91–1.74 (m, 4H). HRMS (ESI+): calcd for  $C_{21}H_{23}BrN_3O_2^+$  [M + H]<sup>+</sup> 428.0968; found 428.0975.

**2-[1-(4-Bromobenzyl)piperidin-4-yl]-3-oxo-2,3-dihydro-1H-isoindole-4-carboxamide (13l).** <sup>1</sup>H NMR (400 MHz, DMSO-*d*<sub>6</sub>)  $\delta$  10.72 (bs, 1H), 8.21 (dd, *J* = 7.4, 1.3 Hz, 1H), 7.76 (dd, *J* = 7.4, 1.3 Hz, 1H), 7.72 (dd, *J* = 7.4, 7.4 Hz, 1H), 7.67 (bs, 1H), 7.53 (d, *J* = 8.3 Hz, 2H), 7.30 (d, *J* = 8.3 Hz, 2H), 4.57 (s, 2H), 4.12–4.01 (m, 1H), 3.49 (s, 2H), 2.94–2.87 (m, 2H), 2.16–2.06 (m, 2H), 1.90–1.71 (m, 4H). HRMS (ESI+): calcd for  $C_{21}H_{23}BrN_3O_2^+$  [M + H]<sup>+</sup> 428.0968; found 428.0983.

**3-Oxo-2-[1-(trifluoromethyl)benzyl)piperidin-4-yl]-2,3-dihydro-1H-isoindole-4-carboxamide (13m).** <sup>1</sup>H NMR (400 MHz, DMSO-*d*<sub>6</sub>)  $\delta$  10.73 (bs, 1H), 8.21 (dd, *J* = 7.6, 1.5 Hz, 1H), 7.85–7.81 (m, 1H), 7.79–7.66 (m, 5H), 7.51–7.46 (m, 1H), 4.59 (s, 2H), 4.15–4.05 (m, 1H), 3.68 (s, 2H), 2.95–2.89 (m, 2H), 2.24–2.16 (m,

2H), 1.92–1.75 (m, 4H). HRMS (ESI+): calcd for  $C_{22}H_{23}F_3N_3O_2^+ [M + H]^+$  418.1737; found 418.1745.

**3-Oxo-2-[1-[3-(trifluoromethyl)benzyl]piperidin-4-yl]-2,3-dihydro-1H-isoindole-4-carboxamide (13n).**  $^1H$  NMR (400 MHz, DMSO- $d_6$ )  $\delta$  10.72 (bs, 1H), 8.21 (dd,  $J$  = 7.4, 1.5 Hz, 1H), 7.77 (dd,  $J$  = 7.5, 1.5 Hz, 1H), 7.73 (dd,  $J$  = 7.5, 7.4 Hz, 1H), 7.70–7.56 (m, SH), 4.59 (s, 2H), 4.13–4.03 (m, 1H), 3.63 (s, 2H), 2.96–2.89 (m, 2H), 2.20–2.10 (m, 2H), 1.91–1.74 (m, 4H). HRMS (ESI+): calcd for  $C_{22}H_{23}F_3N_3O_2^+ [M + H]^+$  418.1737; found 418.1749.

**3-Oxo-2-[1-[4-(trifluoromethyl)benzyl]piperidin-4-yl]-2,3-dihydro-1H-isoindole-4-carboxamide (13o).**  $^1H$  NMR (400 MHz, DMSO- $d_6$ )  $\delta$  10.71 (bs, 1H), 8.20 (dd,  $J$  = 7.4, 1.3 Hz, 1H), 7.76 (dd,  $J$  = 7.6, 1.2 Hz, 1H), 7.74–7.68 (m, 3H), 7.67 (bs, 1H), 7.57 (d,  $J$  = 7.9 Hz, 2H), 4.57 (s, 2H), 4.12–4.02 (m, 1H), 3.61 (s, 2H), 2.96–2.88 (m, 2H), 2.19–2.10 (m, 2H), 1.91–1.72 (m, 4H). HRMS (ESI+): calcd for  $C_{22}H_{23}F_3N_3O_2^+ [M + H]^+$  418.1737; found 418.1740.

**2-[1-{4-(Dimethylamino)benzyl}piperidin-4-yl]-3-oxo-2,3-dihydro-1H-isoindole-4-carboxamide (13p).**  $^1H$  NMR (400 MHz, DMSO- $d_6$ )  $\delta$  10.72 (bs, 1H), 8.19 (dd,  $J$  = 7.4, 1.3 Hz, 1H), 7.76 (dd,  $J$  = 7.5, 1.3 Hz, 1H), 7.71 (t,  $J$  = 7.5, 7.4 Hz, 1H), 7.66 (bs, 1H), 7.11 (d,  $J$  = 8.4 Hz, 2H), 6.69 (d,  $J$  = 8.4 Hz, 2H), 4.55 (s, 2H), 4.09–3.98 (m, 1H), 3.36 (s, 2H), 2.96–2.86 (m, 2H), 2.87 (s, 6H), 2.06–1.97 (m, 2H), 1.86–1.70 (m, 4H). HRMS (ESI+): calcd for  $C_{23}H_{29}N_4O_2^+ [M + H]^+$  393.2285; found 393.2293.

**3-Oxo-2-[1-(pyridin-4-ylmethyl)piperidin-4-yl]-2,3-dihydro-1H-isoindole-4-carboxamide (13q).**  $^1H$  NMR (400 MHz, DMSO- $d_6$ )  $\delta$  10.72 (bs, 1H), 8.54–8.51 (m, 2H), 8.21 (dd,  $J$  = 7.5, 1.4 Hz, 1H), 7.78 (dd,  $J$  = 7.6, 1.4 Hz, 1H), 7.73 (t,  $J$  = 7.6, 7.5 Hz, 1H), 7.68 (bs, 1H), 7.37–7.34 (m, 2H), 4.58 (s, 2H), 4.13–4.03 (m, 1H), 3.56 (s, 2H), 2.95–2.88 (m, 2H), 2.20–2.11 (m, 2H), 1.93–1.74 (m, 4H). HRMS (ESI+): calcd for  $C_{20}H_{23}N_4O_2^+ [M + H]^+$  351.1816; found 351.1817.

**3-Oxo-2-[1-(pyridin-3-ylmethyl)piperidin-4-yl]-2,3-dihydro-1H-isoindole-4-carboxamide (13r).**  $^1H$  NMR (400 MHz, DMSO- $d_6$ )  $\delta$  10.71 (bs, 1H), 8.52 (s, 1H), 8.48 (d,  $J$  = 4.8 Hz, 1H), 8.20 (dd,  $J$  = 7.4, 1.3 Hz, 1H), 7.77–7.71 (m, 3H), 7.66 (bs, 1H), 7.37 (dd,  $J$  = 7.7, 4.8 Hz, 1H), 4.56 (s, 2H), 4.11–4.01 (m, 1H), 3.55 (s, 2H), 2.96–2.87 (m, 2H), 2.19–2.07 (m, 2H), 1.89–1.70 (m, 4H). HRMS (ESI+): calcd for  $C_{20}H_{23}N_4O_2^+ [M + H]^+$  351.1816; found 351.1822.

**3-Oxo-2-[1-(pyridin-2-ylmethyl)piperidin-4-yl]-2,3-dihydro-1H-isoindole-4-carboxamide (13s).**  $^1H$  NMR (400 MHz, DMSO- $d_6$ )  $\delta$  10.73 (bs, 1H), 8.51 (d,  $J$  = 4.8 Hz, 1H), 8.21 (dd,  $J$  = 7.4, 1.3 Hz, 1H), 7.83–7.75 (m, 2H), 7.73 (dd,  $J$  = 7.4, 7.4 Hz, 1H), 7.67 (bs, 1H), 7.47 (d,  $J$  = 7.8 Hz, 1H), 7.28 (dd,  $J$  = 6.8, 4.8 Hz, 1H), 4.58 (s, 2H), 4.14–4.03 (m, 1H), 3.65 (s, 2H), 3.00–2.02 (m, 2H), 2.26–2.14 (m, 2H), 1.93–1.73 (m, 4H). HRMS (ESI+): calcd for  $C_{20}H_{23}N_4O_2^+ [M + H]^+$  351.1816; found 351.1815.

**3-Oxo-2-[1-(thiophen-2-ylmethyl)piperidin-4-yl]-2,3-dihydro-1H-isoindole-4-carboxamide (13t).**  $^1H$  NMR (400 MHz, DMSO- $d_6$ )  $\delta$  10.72 (bs, 1H), 8.21 (dd,  $J$  = 7.4, 1.5 Hz, 1H), 7.77 (dd,  $J$  = 7.5, 1.5 Hz, 1H), 7.72 (dd,  $J$  = 7.5, 7.4 Hz, 1H), 7.67 (bs, 1H), 7.46–7.42 (m, 1H), 7.00–6.97 (m, 2H), 4.58 (s, 2H), 4.11–4.01 (m, 1H), 3.73 (s, 2H), 3.03–2.96 (m, 2H), 2.16–2.08 (m, 2H), 1.88–1.74 (m, 4H). HRMS (ESI+): calcd for  $C_{19}H_{22}N_3O_2S^+ [M + H]^+$  356.1427; found 356.1430.

**3-Oxo-2-[1-(thiophen-3-ylmethyl)piperidin-4-yl]-2,3-dihydro-1H-isoindole-4-carboxamide (13u).**  $^1H$  NMR (400 MHz, DMSO- $d_6$ )  $\delta$  10.73 (bs, 1H), 8.21 (dd,  $J$  = 7.3, 1.3 Hz, 1H), 7.75 (dd,  $J$  = 7.4, 1.3, 1H), 7.72 (dd,  $J$  = 7.4, 7.3 Hz, 1H), 7.67 (bs, 1H), 7.49 (m, 1H), 7.33 (s, 1H), 7.08 (d,  $J$  = 4.6 Hz, 1H), 4.57 (s, 2H), 4.10–3.99 (m, 1H), 3.53 (s, 2H), 2.98–2.90 (m, 2H), 2.12–2.02 (m, 2H), 1.90–1.72 (m, 4H). HRMS (ESI+): calcd for  $C_{19}H_{22}N_3O_2S^+ [M + H]^+$  356.1427; found 356.1432.

**2-[1-(Furan-2-ylmethyl)piperidin-4-yl]-3-oxo-2,3-dihydro-1H-isoindole-4-carboxamide (13v).**  $^1H$  NMR (400 MHz, DMSO- $d_6$ )  $\delta$  10.71 (bs, 1H), 8.19 (dd,  $J$  = 7.4, 1.3 Hz, 1H), 7.76 (dd,  $J$  = 7.5, 1.3 Hz, 1H), 7.71 (dd,  $J$  = 7.5, 7.4 Hz, 1H), 7.66 (bs, 1H), 7.59 (s, 1H), 6.41 (dd,  $J$  = 2.4, 1.8 Hz, 1H), 6.30 (d,  $J$  = 2.4 Hz, 1H), 4.55 (s, 2H), 4.06–3.97 (m, 1H), 3.53 (s, 2H), 2.97–2.89 (m, 2H), 2.15–2.07 (m, 2H), 1.87–1.70 (m, 4H). HRMS (ESI+): calcd for  $C_{19}H_{22}N_3O_3^+ [M + H]^+$  340.1656; found 340.1651.

**2-[1-(Furan-3-ylmethyl)piperidin-4-yl]-3-oxo-2,3-dihydro-1H-isoindole-4-carboxamide (13z).**  $^1H$  NMR (400 MHz, DMSO- $d_6$ )  $\delta$  10.73 (bs, 1H), 8.21 (dd,  $J$  = 7.6, 1.5 Hz, 1H), 7.76 (dd,  $J$  = 7.4, 1.5 Hz, 1H), 7.72 (dd,  $J$  = 7.6, 7.4 Hz, 1H), 7.67 (bs, 1H), 7.58 (s, 1H), 6.45 (s, 1H), 4.56 (s, 2H), 4.11–3.98 (m, 1H), 3.37 (s, 2H), 3.02–2.91 (m, 2H), 2.09–1.99 (m, 2H), 1.88–1.71 (m, 4H). HRMS (ESI+): calcd for  $C_{19}H_{22}N_3O_3^+ [M + H]^+$  340.1656; found 340.1649.

**3-Oxo-2-[1-(1H-pyrrol-2-ylmethyl)piperidin-4-yl]-2,3-dihydro-1H-isoindole-4-carboxamide (13aa).**  $^1H$  NMR (400 MHz, DMSO- $d_6$ )  $\delta$  10.73 (bs, 1H), 10.65 (bs, 1H), 8.20 (dd,  $J$  = 7.4, 1.3 Hz, 1H), 7.77 (dd,  $J$  = 7.6, 1.3 Hz, 1H), 7.72 (dd,  $J$  = 7.6, 7.4 Hz, 1H), 7.67 (bs, 1H), 6.65 (s, 1H), 5.96–5.92 (m, 1H), 5.89 (s, 1H), 4.55 (s, 2H), 4.11–3.97 (m, 1H), 3.44 (s, 2H), 2.99–2.88 (m, 2H), 2.08–1.97 (m, 2H), 1.86–1.71 (m, 4H). HRMS (ESI+): calcd for  $C_{19}H_{23}N_4O_2^+ [M + H]^+$  339.1816; found 339.1812.

**2-[1-(1-Methyl-1H-pyrrol-2-yl)methyl)piperidin-4-yl]-3-oxo-2,3-dihydro-1H-isoindole-4-carboxamide (13ab).**  $^1H$  NMR (400 MHz, DMSO- $d_6$ )  $\delta$  10.72 (bs, 1H), 8.19 (dd,  $J$  = 7.3, 1.5 Hz, 1H), 7.75 (dd,  $J$  = 7.4, 1.2 Hz, 1H), 7.71 (dd,  $J$  = 7.4, 7.3 Hz, 1H), 7.66 (bs, 1H), 6.67–6.65 (m, 1H), 5.89–5.85 (m, 2H), 4.55 (s, 2H), 4.10–4.00 (m, 1H), 3.61 (s, 3H), 3.41 (s, 2H), 2.98–2.89 (m, 2H), 2.07–1.97 (m, 2H), 1.80–1.70 (m, 4H). HRMS (ESI+): calcd for  $C_{20}H_{25}N_4O_2^+ [M + H]^+$  353.1972; found 353.1984.

**2-[1-(1H-Indol-4-ylmethyl)piperidin-4-yl]-3-oxo-2,3-dihydro-1H-isoindole-4-carboxamide (13ac).**  $^1H$  NMR (400 MHz, DMSO- $d_6$ )  $\delta$  11.06 (bs, 1H), 10.74 (bs, 1H), 8.20 (dd,  $J$  = 7.4, 1.5 Hz, 1H), 7.75 (dd,  $J$  = 7.5, 1.2 Hz, 1H), 7.72 (dd,  $J$  = 7.5, 7.4 Hz, 1H), 7.67 (bs, 1H), 7.35–7.28 (m, 2H), 7.08–7.02 (m, 1H), 6.99–6.94 (m, 1H), 6.61 (s, 1H), 4.57 (s, 2H), 4.13–4.02 (m, 1H), 3.75 (s, 2H), 3.04–2.96 (m, 2H), 2.19–2.09 (m, 2H), 1.89–1.71 (m, 4H). HRMS (ESI+): calcd for  $C_{23}H_{25}N_4O_2^+ [M + H]^+$  389.1972; found 389.1983.

**2-[1-(1H-Indol-5-ylmethyl)piperidin-4-yl]-3-oxo-2,3-dihydro-1H-isoindole-4-carboxamide (13ad).**  $^1H$  NMR (400 MHz, DMSO- $d_6$ )  $\delta$  11.01 (bs, 1H), 10.73 (bs, 1H), 8.20 (dd,  $J$  = 7.3, 1.5 Hz, 1H), 7.75 (dd,  $J$  = 7.4, 1.5 Hz, 1H), 7.71 (dd,  $J$  = 7.4, 7.3 Hz, 1H), 7.66 (bs, 1H), 7.46 (s, 1H), 7.34 (d,  $J$  = 8.2 Hz, 1H), 7.33–7.28 (m, 1H), 7.07 (dd,  $J$  = 8.2, 1.3 Hz, 1H), 6.40–6.37 (m, 1H), 4.56 (s, 2H), 4.10–4.00 (m, 1H), 3.56 (s, 2H), 3.00–2.92 (m, 2H), 2.13–2.02 (m, 2H), 1.87–1.71 (m, 4H). HRMS (ESI+): calcd for  $C_{23}H_{25}N_4O_2^+ [M + H]^+$  389.1972; found 389.1970.

**3-Oxo-2-[1-(tetrahydro-2H-pyran-4-yl)piperidin-4-yl]-2,3-dihydro-1H-isoindole-4-carboxamide (13ae).**  $^1H$  NMR (400 MHz, DMSO- $d_6$ )  $\delta$  10.74 (bs, 1H), 8.20 (dd,  $J$  = 7.6, 1.5 Hz, 1H), 7.76 (dd,  $J$  = 7.4, 1.5 Hz, 1H), 7.71 (dd,  $J$  = 7.6, 7.4 Hz, 1H), 7.66 (bs, 1H), 4.55 (s, 2H), 4.07–3.98 (m, 1H), 3.92–3.85 (m, 2H), 3.35–3.24 (m partially overlapped by water signal, 2H), 3.04–2.96 (m, 2H), 2.47–2.42 (m partially overlapped by DMSO signal, 1H), 2.29–2.19 (m, 2H), 1.81–1.65 (m, 6H), 1.50–1.38 (m, 2H). HRMS (ESI+): calcd for  $C_{19}H_{26}N_3O_3^+ [M + H]^+$  344.1969; found 344.1962.

**2-[1-(1,4-Dioxaspiro[4.5]dec-8-yl)piperidin-4-yl]-3-oxo-2,3-dihydro-1H-isoindole-4-carboxamide (13ag).**  $^1H$  NMR (400 MHz, DMSO- $d_6$ )  $\delta$  10.74 (bs, 1H), 8.20 (dd,  $J$  = 7.4, 1.5 Hz, 1H), 7.76 (dd,  $J$  = 7.6, 1.5 Hz, 1H), 7.71 (dd,  $J$  = 7.6, 7.4 Hz, 1H), 7.66 (bs, 1H), 4.55 (s, 2H), 4.05–3.95 (m, 1H), 3.86–3.80 (m, 4H), 2.97–2.89 (m, 2H), 2.44–2.34 (m, 1H), 2.33–2.23 (m, 2H), 1.80–1.37 (m, 12H). HRMS (ESI+): calcd for  $C_{22}H_{30}N_3O_4^+ [M + H]^+$  400.2231; found 400.2229.

**4-Fluoro-2-iodo-6-methyl-benzoic Acid (15b).** A mixture of 4-fluoro-2-methyl-benzoic acid 14b (20.00 g, 0.130 mol), iodobenzene diacetate (50.15 g, 0.156 mol), iodine (39.52 g, 0.156 mol), and palladium(II) acetate (1.46 g, 0.006 mol) in *N,N*-dimethylformamide (360 mL) was degassed by cycling vacuum and nitrogen three times and was then heated for 18 h at 100 °C internal temperature, under argon. The resulting dark mixture was cooled to room temperature, diluted with methyl-*tert*-butylether (200 mL), and treated with a solution of sodium metabisulfite (250 g) in water (500 mL) under efficient stirring. Then, this yellow colored mixture was acidified by slowly adding conc hydrochloric acid (130 mL). The aqueous layer was separated and extracted twice with methyl-*tert*-butylether (100 mL × 2).

The combined organic extracts were treated with a solution of sodium hydroxide pellets (80 g) in water (300 mL) under stirring. The organic layer containing only iodobenzene was discarded, while the aqueous layer was added with sodium chloride, cooled to ice temperature, and brought to pH = 1 with conc hydrochloric acid (130 mL). From this aqueous medium, the product was extracted with methyl-*tert*-butylether (100 mL × 3) and the combined extracts were dried over Na<sub>2</sub>SO<sub>4</sub> and finally concentrated under reduced pressure, affording the title compound (30.5 g, 84%) as brown solid. This raw material was used in the next step without purification. <sup>1</sup>H NMR (400 MHz, CDCl<sub>3</sub>) δ 7.45 (dd, J<sub>HH</sub> = 2.4 Hz, J<sub>HF</sub> = 7.9, 1H), 6.96 (dd, J<sub>HH</sub> = 2.4 Hz, J<sub>HF</sub> = 9.1, 1H), 2.46 (s, 3H). ESI(+) MS: m/z 281 (MH<sup>+</sup>).

**Compounds 15a, 15c, 15d.** Operating in an analogous way but employing suitably substituted starting material, the following compounds were obtained:

**3-Fluoro-2-iodo-6-methylbenzoic Acid (15a).** <sup>1</sup>H NMR (400 MHz, DMSO-d<sub>6</sub>) δ 13.69 (bs, 1H), 7.30 (dd, J<sub>HH</sub> = 8.9 Hz, J<sub>HF</sub> = 5.6 Hz, 1H), 7.19 (dd, J<sub>HH</sub> = 8.9 Hz, J<sub>HF</sub> = 8.2 Hz, 1H), 2.27 (s, 3H). ESI(+) MS: m/z 281 (MH<sup>+</sup>).

**3-Fluoro-6-iodo-2-methylbenzoic Acid (15c).** <sup>1</sup>H NMR (400 MHz, DMSO-d<sub>6</sub>) δ 7.71 (dd, J<sub>HH</sub> = 9.0 Hz, J<sub>HF</sub> = 5.0 Hz, 1H), 7.04 (dd, J<sub>HH</sub> = 9.0 Hz, J<sub>HF</sub> = 9.3 Hz, 1H), 2.20 (d, J<sub>HF</sub> = 2.2 Hz, 3H). ESI(+) MS: m/z 281 (MH<sup>+</sup>).

**4-Chloro-2-iodo-6-methylbenzoic Acid (15d).** <sup>1</sup>H NMR (400 MHz, DMSO-d<sub>6</sub>) δ 7.83–7.81 (m, 1H), 7.47–7.45 (m, 1H), 2.25 (s, 3H). ESI(+) MS: m/z 297 (MH<sup>+</sup>).

**4-Fluoro-2-iodo-6-methylbenzoic Acid Methyl Ester (16b).** To a solution of **15b** (30.05 g, 0.109 mol) in *N,N*-dimethylformamide (300 mL) was added anhydrous potassium carbonate (22.0 g, 0.16 mol) under efficient magnetic stirring. After 15 min, methyl *p*-toluenesulfonate (30.7 g, 0.16 mol) was added. The brown suspension was stirred at room temperature for 2 h. Potassium acetate (12.4 g, 0.13 mol) was then added to destroy the unreacted methyl *p*-toluenesulfonate, and the mixture was stirred overnight. The thick reaction mixture was diluted with methyl-*tert*-butylether (100 mL) and washed with water (600 mL); the aqueous layer was separated and extracted twice with methyl-*tert*-butylether (70 mL × 2). The combined organic extracts were washed with brine (50 mL), dried over Na<sub>2</sub>SO<sub>4</sub>, and concentrated under reduced pressure to a solid residue. This material was purified by flash chromatography (*n*-hexane/ethyl acetate 9:1), affording the desired compound (26.2 g, 81%) as colorless oil. <sup>1</sup>H NMR (400 MHz, DMSO-d<sub>6</sub>) δ 7.63 (dd, J<sub>HH</sub> = 2.4 Hz, J<sub>HF</sub> = 8.3 Hz, 1H), 7.25 (dd, J<sub>HH</sub> = 2.4 Hz, J<sub>HF</sub> = 9.6 Hz, 1H), 3.86 (s, 3H), 2.27 (s, 3H). ESI(+) MS: m/z 295 (MH<sup>+</sup>).

**Compounds 16a, 16c, 16d.** Operating in an analogous way but employing suitably substituted starting material, the following compounds were obtained:

**Methyl 3-Fluoro-2-iodo-6-methylbenzoate (16a).** <sup>1</sup>H NMR (400 MHz, DMSO-d<sub>6</sub>) δ 7.29 (dd, J<sub>HH</sub> = 8.4 Hz, J<sub>HF</sub> = 5.2 Hz, 1H), 7.25 (dd, J<sub>HH</sub> = 8.4 Hz, J<sub>HF</sub> = 8.0 Hz, 1H), 3.89 (s, 3H), 2.24 (s, 3H). ESI(+) MS: m/z 295 (MH<sup>+</sup>).

**Methyl 3-Fluoro-6-iodo-2-methylbenzoate (16c).** <sup>1</sup>H NMR (400 MHz, DMSO-d<sub>6</sub>) δ 7.75 (dd, J<sub>HH</sub> = 8.7 Hz, J<sub>HF</sub> = 5.0 Hz, 1H), 7.11 (dd, J<sub>HH</sub> = 8.7 Hz, J<sub>HF</sub> = 9.5 Hz, 1H), 3.89 (s, 3H), 2.16 (d, J<sub>HF</sub> = 2.3 Hz, 3H). ESI(+) MS: m/z 295 (MH<sup>+</sup>).

**Methyl 4-Chloro-2-iodo-6-methylbenzoate (16d).** <sup>1</sup>H NMR (400 MHz, DMSO-d<sub>6</sub>) δ 7.82 (m, 1H), 7.46 (m, 1H), 3.87 (s, 3H), 2.25 (s, 3H). ESI(+) MS: m/z 311 (MH<sup>+</sup>).

**2-[1-(4,4-Difluorocyclohexyl)piperidin-4-yl]-5-fluoro-7-iodo-2,3-dihydro-1*H*-isoindol-1-one (18by).** To a solution of **16b** (2.2 g, 7.5 mmol) in methyl pivalate (13 mL), *N*-bromosuccinimide (2.2 g, 12.3 mmol) and benzoylperoxide (146 mg, 0.78 mmol) were added. The reaction mixture was stirred at 85 °C under nitrogen atmosphere for 3 h. Crude was filtered on Gooch and washed with toluene. Volatiles were evaporated, and the residue was dissolved in acetonitrile (21 mL). Triethylamine (2.8 mL, 20.4 mmol) and **17y** (1.5 g, 6.8 mmol) were added, and the reaction mixture was stirred at 90 °C for 4 h. Crude was diluted with dichloromethane and washed with 15% ammonium hydroxide. The organic phase was dried over sodium sulfate, filtered, and evaporated. Column chromatography (dichloromethane/ethanol: 95/5)

afforded title compound (1.9 g, 58%). <sup>1</sup>H NMR (400 MHz, DMSO-d<sub>6</sub>) δ 7.80 (dd, J<sub>HH</sub> = 2.2 Hz, J<sub>HF</sub> = 8.9 Hz, 1H), 7.51 (dd, J<sub>HH</sub> = 2.2 Hz, J<sub>HF</sub> = 8.3 Hz, 1H), 4.37 (s, 2H), 4.02–3.89 (m, 1H), 2.99–2.88 (m, 2H), 2.54–2.45 (m overlapped by DMSO signal, 1H), 2.33–2.21 (m, 2H), 2.10–1.97 (m, 2H), 1.90–1.67 (m, 8H), 1.61–1.47 (m, 2H). HRMS (ESI+): calcd for C<sub>19</sub>H<sub>22</sub>F<sub>3</sub>IN<sub>2</sub>O<sup>+</sup> [M + H]<sup>+</sup> 479.0802; found 479.0803.

**Compounds 18ay, 18cy, and 18dy.** Operating in an analogous way but employing suitably substituted starting material, the following compounds were obtained:

**2-[1-(4,4-Difluorocyclohexyl)piperidin-4-yl]-6-fluoro-7-iodo-2,3-dihydro-1*H*-isoindol-1-one (18ay).** <sup>1</sup>H NMR (400 MHz, DMSO-d<sub>6</sub>) δ 7.57 (dd, J<sub>HH</sub> = 8.2 Hz, J<sub>HF</sub> = 4.6 Hz, 1H), 7.45 (dd, J<sub>HH</sub> = 8.2 Hz, J<sub>HF</sub> = 8.4 Hz, 1H), 4.36 (s, 2H), 4.02–3.92 (m, 1H), 2.98–2.90 (m, 2H), 2.54–2.45 (m overlapped by DMSO signal, 1H), 2.32–2.22 (m, 2H), 2.10–1.96 (m, 2H), 1.91–1.69 (m, 8H), 1.60–1.48 (m, 2H). HRMS (ESI+): calcd for C<sub>19</sub>H<sub>22</sub>F<sub>3</sub>IN<sub>2</sub>O<sup>+</sup> [M + H]<sup>+</sup> 479.0802; found 479.0790.

**2-[1-(4,4-Difluorocyclohexyl)piperidin-4-yl]-4-fluoro-7-iodo-2,3-dihydro-1*H*-isoindol-1-one (18cy).** <sup>1</sup>H NMR (400 MHz, DMSO-d<sub>6</sub>) δ 7.92 (dd, J<sub>HH</sub> = 8.5 Hz, J<sub>HF</sub> = 4.5 Hz, 1H), 7.24 (dd, J<sub>HH</sub> = 8.5 Hz, J<sub>HF</sub> = 8.7 Hz, 1H), 4.47 (s, 2H), 4.01–3.90 (m, 1H), 2.97–2.90 (m, 2H), 2.54–2.45 (m overlapped by DMSO signal, 1H), 2.31–2.22 (m, 2H), 2.11–1.93 (m, 2H), 1.92–1.67 (m, 8H), 1.61–1.48 (m, 2H). HRMS (ESI+): calcd for C<sub>19</sub>H<sub>23</sub>F<sub>3</sub>IN<sub>2</sub>O<sup>+</sup> [M + H]<sup>+</sup> 479.0802; found 479.0804.

**2-[1-(4,4-Difluorocyclohexyl)piperidin-4-yl]-5-chloro-7-iodo-2,3-dihydro-1*H*-isoindole-4-carbonitrile (18dy).** ESI(+) MS: m/z 495 (MH<sup>+</sup>). After HPLC-MS analysis, compound **18dy** was submitted to the next step without further purification and <sup>1</sup>H NMR characterization.

**2-[1-(4,4-Difluorocyclohexyl)piperidin-4-yl]-6-fluoro-3-oxo-2,3-dihydro-1*H*-isoindole-4-carbonitrile (19by).** **18by** (1.9 g, 3.97 mmol) and copper(I) cyanide (534 mg, 5.96 mmol) were dissolved in *N,N*-dimethylformamide (16 mL), and the resulted solution was refluxed under nitrogen atmosphere for 3 h. The solvent was removed under reduced pressure, and the residue was diluted with dichloromethane and washed with 15% ammonium hydroxide. Organic phase was dried over sodium sulfate, filtered, and evaporated. Column chromatography (dichloromethane/ethanol: 95/5) afforded title compound (1.28 g, 86%). <sup>1</sup>H NMR (400 MHz, DMSO-d<sub>6</sub>) δ 7.95 (dd, J<sub>HH</sub> = 2.2 Hz, J<sub>HF</sub> = 9.2 Hz, 1H), 7.83 (dd, J<sub>HH</sub> = 2.2 Hz, J<sub>HF</sub> = 8.3 Hz, 1H), 4.49 (m, 2H), 3.98–3.89 (m, 1H), 2.98–2.86 (m, 2H), 2.51–2.41 (m overlapped by DMSO signal, 1H), 2.33–2.19 (m, 2H), 2.07–1.92 (m, 2H), 1.90–1.64 (m, 8H), 1.58–1.43 (m, 2H). HRMS (ESI+): calcd for C<sub>20</sub>H<sub>23</sub>F<sub>3</sub>N<sub>3</sub>O<sup>+</sup> [M + H]<sup>+</sup> 378.1788; found 378.1782.

**Compounds 19ay, 19cy, and 19dy.** Operating in an analogous way but employing suitably substituted starting material, the following compounds were obtained:

**2-[1-(4,4-Difluorocyclohexyl)piperidin-4-yl]-5-fluoro-3-oxo-2,3-dihydro-1*H*-isoindole-4-carbonitrile (19ay).** <sup>1</sup>H NMR (400 MHz, DMSO-d<sub>6</sub>) δ 7.98 (dd, J<sub>HH</sub> = 8.5 Hz, J<sub>HF</sub> = 4.6 Hz, 1H), 7.74 (dd, J<sub>HH</sub> = 8.5 Hz, J<sub>HF</sub> = 9.8 Hz, 1H), 4.51 (s, 2H), 4.02–3.92 (m, 1H), 2.97–2.90 (m, 2H), 2.54–2.45 (m overlapped by DMSO signal, 1H), 2.34–2.23 (m, 2H), 2.11–1.96 (m, 2H), 1.93–1.67 (m, 8H), 1.61–1.48 (m, 2H). HRMS (ESI+): calcd for C<sub>20</sub>H<sub>23</sub>F<sub>3</sub>N<sub>3</sub>O<sup>+</sup> [M + H]<sup>+</sup> 378.1788; found 378.1779.

**7-Fluoro-2-[1-(4,4-difluorocyclohexyl)piperidin-4-yl]-3-oxo-2,3-dihydro-1*H*-isoindole-4-carbonitrile (19cy).** <sup>1</sup>H NMR (400 MHz, DMSO-d<sub>6</sub>) δ 8.05 (dd, J<sub>HH</sub> = 8.5 Hz, J<sub>HF</sub> = 4.3 Hz, 1H), 7.65 (dd, J<sub>HH</sub> = 8.5 Hz, J<sub>HF</sub> = 8.7 Hz, 1H), 4.62 (s, 2H), 4.02–3.92 (m, 1H), 2.97–2.90 (m, 2H), 2.54–2.45 (m overlapped by DMSO signal, 1H), 2.34–2.24 (m, 2H), 2.11–1.96 (m, 2H), 1.93–1.67 (m, 8H), 1.61–1.48 (m, 2H). ESI(+) MS: m/z 378 (MH<sup>+</sup>).

**6-Chloro-2-[1-(4,4-difluorocyclohexyl)piperidin-4-yl]-3-oxo-2,3-dihydro-1*H*-isoindole-4-carbonitrile (19dy).** <sup>1</sup>H NMR (400 MHz, DMSO-d<sub>6</sub>) δ 8.15 (d, J = 1.8 Hz, 1H), 8.06 (d, J = 1.8 Hz, 1H), 4.52 (s, 2H), 4.01–3.91 (m, 1H), 2.97–2.90 (m, 2H), 2.33–2.22 (m, 2H), 2.10–1.96 (m, 8H), 1.63–1.46 (m, 2H). HRMS (ESI+): calcd for C<sub>20</sub>H<sub>23</sub>ClF<sub>3</sub>N<sub>3</sub>O<sup>+</sup> [M + H]<sup>+</sup> 394.1492; found 394.1502.

**2-[1-(4,4-Difluorocyclohexyl)-piperidin-4-yl]-6-fluoro-3-oxo-2,3-dihydro-1*H*-isoindole-4-carboxamide (20by).** To a solution of

**19by** (2.81 g; 7.44 mmol) in toluene (28 mL), acetaldoxime (4.4 g; 74.4 mmol) and indium(III) chloride (82 mg; 0.37 mmol) were added at room temperature. The resulting solution was heated at reflux for 1 h then concentrated under reduced pressure. The residue was taken up with water, 2-propanol, and dichloromethane. The organic layer was separated and finally concentrated under reduced pressure. The resulting crude was crystallized from ethanol, delivering, after drying, the desired compound (1.82 g, 62%) as a white solid. <sup>1</sup>H NMR (400 MHz, DMSO-*d*<sub>6</sub>) δ 10.77 (bs, 1H), 7.89 (dd, *J*<sub>HH</sub> = 2.6 Hz, *J*<sub>HF</sub> = 10.9 Hz, 1H), 7.85 (bs, 1H), 7.66 (dd, *J*<sub>HH</sub> = 2.6 Hz, *J*<sub>HF</sub> = 7.7 Hz, 1H), 4.56 (s, 2H), 4.04–3.94 (m, 1H), 2.98–2.91 (m, 2H), 2.53–2.45 (m, overlapped by DMSO signal, 1H), 2.32–2.22 (m, 2H), 2.10–1.96 (m, 2H), 1.92–1.67 (m, 8H), 1.60–1.48 (m, 2H). HRMS (ESI+): calcd for C<sub>20</sub>H<sub>25</sub>F<sub>3</sub>N<sub>3</sub>O<sub>2</sub><sup>+</sup> [M + H]<sup>+</sup> 396.1894; found 396.1890.

**Compounds 20ay, 20cy, and 20dy.** Operating in an analogous way but employing suitably substituted starting material, the following compounds were obtained:

**2-[1-(4,4-Difluorocyclohexyl)piperidin-4-yl]-5-fluoro-3-oxo-2,3-dihydro-1H-isoindole-4-carboxamide (20ay).** <sup>1</sup>H NMR (400 MHz, DMSO-*d*<sub>6</sub>) δ 7.86 (bs, 1H), 7.62 (bs, 1H), 7.59 (dd, *J*<sub>HH</sub> = 8.4 Hz, *J*<sub>HF</sub> = 4.5 Hz, 1H), 7.44 (dd, *J*<sub>HH</sub> = 8.4 Hz, *J*<sub>HF</sub> = 9.6 Hz, 1H), 4.42 (s, 2H), 3.99–3.89 (m, 1H), 2.97–2.90 (m, 2H), 2.53–2.45 (m overlapped by DMSO signal, 1H), 2.32–2.23 (m, 2H), 2.10–1.96 (m, 2H), 1.91–1.66 (m, 8H), 1.61–1.46 (m, 2H). HRMS (ESI+): calcd for C<sub>20</sub>H<sub>25</sub>F<sub>3</sub>N<sub>3</sub>O<sub>2</sub><sup>+</sup> [M + H]<sup>+</sup> 396.1894; found 396.1884.

**2-[1-(4,4-Difluorocyclohexyl)piperidin-4-yl]-7-fluoro-3-oxo-2,3-dihydro-1H-isoindole-4-carboxamide (20cy).** <sup>1</sup>H NMR (400 MHz, DMSO-*d*<sub>6</sub>) δ 10.55 (bs, 1H), 8.26 (dd, *J*<sub>HH</sub> = 8.8 Hz, *J*<sub>HF</sub> = 5.2 Hz, 1H), 7.71 (bs, 1H), 7.57 (dd, *J*<sub>HH</sub> = 8.8 Hz, *J*<sub>HF</sub> = 8.4 Hz, 1H), 4.63 (s, 2H), 4.06–3.95 (m, 1H), 2.99–2.91 (m, 2H), 2.56–2.44 (m overlapped by DMSO signal, 1H), 2.34–2.22 (m, 2H), 2.09–1.97 (m, 2H), 1.93–1.71 (m, 8H), 1.61–1.48 (m, 2H). HRMS (ESI+): calcd for C<sub>20</sub>H<sub>25</sub>F<sub>3</sub>N<sub>3</sub>O<sub>2</sub><sup>+</sup> [M + H]<sup>+</sup> 396.1894; found 396.1900.

**6-Chloro-2-[1-(4,4-difluorocyclohexyl)piperidin-4-yl]-3-oxo-2,3-dihydro-1H-isoindole-4-carboxamide (20dy).** <sup>1</sup>H NMR (400 MHz, DMSO-*d*<sub>6</sub>) δ 10.68 (bs, 1H), 8.12 (d, *J* = 2.1 Hz, 1H), 7.89 (d, *J* = 2.1 Hz, 1H), 7.86 (bs, 1H), 4.56 (s, 2H), 4.05–3.95 (m, 1H), 2.98–2.91 (m, 2H), 2.54–2.45 (m overlapped by DMSO signal, 1H), 2.32–2.23 (m, 2H), 2.10–1.97 (m, 2H), 1.91–1.68 (m, 8H), 1.61–1.48 (m, 2H). HRMS (ESI+): calcd for C<sub>20</sub>H<sub>25</sub>ClF<sub>3</sub>N<sub>3</sub>O<sub>2</sub><sup>+</sup> [M + H]<sup>+</sup> 412.1598; found 412.159.

**2. Biochemistry.** **2.1. Protein Production.** PARP-1 full length (FL) and catalytic domain (CD), PARP-2 FL and CD, PARP-3 FL, and TNKS-1 CD were prepared as previously described.<sup>21</sup>

**2.2. Fluorescence Polarization Displacement Assay.** Fluorescence polarization displacement assay on PARP-1 FL, PARP-2 FL, PARP-3 FL, and TNKS-1 CD was performed as reported.<sup>21</sup>

**2.3. Surface Plasmon Resonance Binding Assay.** Surface plasmon resonance binding assay on PARP-1 CD and on PARP-2 CD was conducted as previously reported.<sup>21</sup>

**2.4. Kinase Assay.** Compound **20by** was profiled as previously described<sup>45</sup> on 56 different kinases (ABL, ACK1, AKT1, ALK, AUR1, AUR2, BRK, BUB1, CDC7/DBF4, CDK2/CYCA, CHK1, CK2, EEF2K, EGFR1, ERK2, EphA2, FAK, FGFR1, FLT3, GSK3beta, Haspin, IGFR1, IKK2, IR, JAK1, JAK2, KIT, LCK, LYN, MAPKAPK2, MELK, MET, MNK2, MPS1, MST4, NEK6, NIM1, P38alpha, PAK4, PDGFRb, PDK1, PERK, PIM1, PIM2, PKAalpha, PKCbeta, PLK1, RET, SULU1, Syk, TLK2, TRKA, TYK2, VEGFR2, ZAP70). The IC<sub>50</sub> values were found to be >10 μM for all enzymes tested.

**2.5. HTS Campaign.** See ref 21 for HTS experimental details.

**3. Cell Biology.** **3.1. PAR Assay.** Cellular activity of PARP-1 inhibitors was assessed by measuring the inhibition of the hydrogen peroxide induced PAR formation in HeLa cells (ECACC). Cellular PAR levels were measured by immunocytochemistry and quantified using an ArrayScan vTi instrument (Cellomics Thermo Scientific).

Studies were performed as follows: 6000 cells/well were seeded in 96-well plates (PerkinElmer) in MEM/10% FCS and incubated for 24 h at 37 °C, 5% carbon dioxide. Test compounds were then added at the required concentration for 30 min. DNA damage was then induced

by adding hydrogen peroxide at the concentration of 0.1 mM for 15 min. Concentration curves were prepared in MEM/10% FCS from compound stocks in DMSO, and final DMSO concentration was 0.002% (v/v). Duplicate wells for each concentration point were prepared with a typical highest compound concentration of 20 μM and serial dilution 1:3. Plates were dried and fixed by adding cold methanol-acetone (70:30) solution for 15 min at room temperature, fixing solution was aspirated, and wells were air-dried for 5 min and then dehydrated in PBS. Nonspecific binding sites were blocked by incubating wells for 30 min in PBS containing 5% (w/v) FBS 0.05% Tween 20. Wells were then incubated for 1 h at room temperature in PBS containing anti-PAR mouse monoclonal antibody (Anti-PAR, mouse mAb 10H, Tulip Catalogue no. 1020) diluted 1:200 in blocking solution. After three washes in PBS, wells incubated in PBS (w/v) 5% FBS 0.05% Tween 20 containing 2 μg/mL Cy2-conjugated Goat anti-mouse secondary antibody (Amersham Pharmacia Biotech catalogue no. PA 42002) (absorption maximum 489 nm fluorescence maximum 506 nm) and 1 μg/mL DAPI (4',6-diamidino-2-phenylindole dilactate, absorption maximum 359 nm fluorescence maximum 461 nm, Sigma catalogue no. D9564). After washing further three times in PBS, cellular PAR immunoreactivity was assessed using the ArrayScan vTi instrument, with a Zeiss 10× 0.5 NA objective and applying the CytoNucTrans V3 algorithm (Cellomics/Thermo Fisher) with a XF100 filter. At least 10 fields, corresponding to at least 900 cells, were read for each well. Compound IC<sub>50</sub>s were derived from sigmoidal interpolation functions of experimental data using GraphPad Prism software.

**3.2. Colony Forming Assay.** Inhibition of cell proliferation was evaluated as follows: cells were seeded at a density of 600 cells/cm<sup>2</sup> in RPMI medium, supplemented with 10% FBS. After 24 h, medium was replaced with the same containing increasing serial dilutions of inhibitor starting from a highest concentration of 10 μM. After 10 days, cells were fixed and stained with crystal violet. Colonies were counted using Infrared Scanner (Odyssey Li-Cor). All the experiments were performed in duplicate. IC<sub>50</sub> was calculated using the GraphPad Prism software.<sup>46</sup>

**4. X-ray Crystallographic Data.** Crystals of the catalytic domain of hPARP-1 in complex with compound **10b** and **20by** were grown at 4 °C using the vapor diffusion method from a solution of 2 M ammonium sulfate, 2% Peg 400, and 0.1 M Tris, pH 8. Before crystallization, the protein was concentrated at 10 mg/mL in a buffer containing 50 mM TrisHCl, pH 8.0, 150 mM sodium chloride, 10% glycerol, 14 mM β-mercaptoethanol, and 0.1% β-octylglucoside. Compounds **10b** and **20by** were added to the protein solution at a final concentration of 0.5 mM. Small cocrystals of **10b** grew in a few days and were optimized using streak seeding. On the contrary, the catalytic domain of hPARP-1 in complex with **20by** crystallized only after several months, giving a different crystal form (space group of hPARP-1–**20by** crystal is I222, while for hPARP-1–**10b** crystal is C2). For data collection, crystals were cryoprotected in a mother liquor solution containing 30% glycerol and frozen in liquid nitrogen. Crystals of the catalytic domain of hPARP-2 in complex with compounds **10b** and **20by** were obtained at 4 °C by the vapor diffusion method (hanging drops), mixing equal volumes of a protein solution (10 mg/mL of protein in 50 mM TrisHCl, pH 8.5, 150 mM sodium chloride, and 0.5 mM dithiothreitol (DTT) containing either **10b** or **20by** at a final concentration of 0.5 mM) and the reservoir solution consisting of 25% PEG 4000, 0.2 M magnesium chloride, and 0.1 M TrisHCl, pH 8.5. Addition of 0.1% β-octylglucoside and streak seeding improved the quality and reproducibility of the crystals. Crystals were further transferred to a cryoprotectant solution (reservoir solution supplemented with 30% glycerol) and frozen in liquid nitrogen. Diffraction data for the different complexes were collected at ESRF (Grenoble, France). Data were indexed and integrated using Mosflm and Scala,<sup>47,48</sup> structures were refined with Refmac,<sup>48,49</sup> and model building was performed with Coot.<sup>50</sup> All structures have been deposited to the Protein Data Bank (PDB) with accession codes: 4ZZX, 4ZZY, 4ZZZ, and 5A00.

**5. ADME Data.** **5.1. Solubility.** Solubility at pH = 7 was measured as previously reported.<sup>51</sup>

**5.2. Cell Permeability.** PAMPA permeability assay was performed as described.<sup>51</sup>

**5.3. Plasma Protein Binding.** Plasma protein binding was evaluated according to the methodology already described.<sup>52</sup>

**5.4. Intrinsic Clearance in Human Liver Microsomes (HLM).** Metabolic stability in the presence of human liver microsomes was assessed as reported.<sup>51</sup>

**5.5. Intrinsic Clearance in Rat Hepatocytes.** Clearance determination in rat hepatocytes was performed as previously described.<sup>51</sup>

**6. In Vivo Pharmacokinetic Studies.** All procedures adopted for housing and handling of animals were in strict compliance with Italian and European guidelines for Laboratory Animal Welfare and the protocols were approved by IRB.

**6.1. Pharmacokinetics in Mouse.** The pharmacokinetic profile and the oral bioavailability of the compounds have been investigated in mouse (Balb, Nu/Nu, Harlan, Italy) in ad hoc pharmacokinetic studies. The compounds were formulated for intravenous bolus administration as follows: 5% Tween 80 in 5% dextrose for **13i**; PEG 400 in 5% dextrose for **13ad**; 10% Tween 80 in 5% dextrose for **13af** and **20by**. Oral administration was performed by using the compounds formulated in 0.5% methylcellulose. A single administration at the dose of 10 mg/kg was given, and three male animals for each route were used. All blood samples were taken from retro-orbital vein at 5 min, 30 min, 1 h, 3 h, 6 h, and 24 h after intravenous administration and 15 min, 30 min, 1 h, 3 h, 6 h, and 24 h after oral administration. Plasma samples were prepared by plasma proteins precipitation by adding 200 μL of acetonitrile to 20 μL of plasma in a 96-well plate. After capping and vortex mixing, the plate was centrifuged for 15 min at 4000 rpm. The supernatant was considered as final extract and injected onto the LC-MS/MS system (UHPLC system, Waters Acquity using BEH HILIC 50 mm × 2.1 mm 1.7 μm analytical column; MS instrument, Waters TQD equipped with electrospray ion source operating in positive ion mode). Lower limit of quantification is 5.0 ng/mL, and upper limit of quantification is 5000 ng/mL. Pharmacokinetic analysis was performed with WinNonlin software (version 5.2.1) using a noncompartmental method (linear trapezoidal rule and linear regression analysis of natural log-transformed plasma concentrations vs time data). Oral bioavailability (*F*) was calculated from the ratio of average oral to IV (intravenous) dose-normalized plasma AUC values.

**6.2. Pharmacokinetics in Rat.** The pharmacokinetic profile and the oral bioavailability of the compounds have been investigated in rat (Sprague–Dawley, Charles River Laboratories, Italy) in ad hoc pharmacokinetic studies. Compound **20by** was formulated for intravenous bolus administration in 20% DMSO + 40% PEG 400 in 5% dextrose. Oral administration was performed by using a **20by** suspension in 0.5% methylcellulose. A single administration at the dose of 10 mg/kg for each route, and a single oral administration at the dose of 100 mg/kg were given. Three male animals for each study were used. All blood samples were taken by means of a cannula implanted in the superior vena cava via the jugular vein at 5 min, 30 min, 1 h, 3 h, 6 h, and 24 h after intravenous administration and 15 min, 30 min, 1 h, 3 h, 6 h, and 24 h after oral administration. Plasma samples were prepared by plasma proteins precipitation by adding 200 μL of acetonitrile to 20 μL of plasma in a 96-well plate. After capping and vortex mixing, the plate was centrifuged for 15 min at 3700 rpm at 6 °C. The supernatant was considered as final extract and injected onto the LC-MS/MS system (HPLC system, Hewlett-Packard 1100 series using Zorbax SB CN 75 mm × 4.6 mm 3.5 μm analytical column; MS instrument, MDS/SCIEX 4000QTRAP equipped with TURBO ION SPRAY source operating in positive ion mode). Lower limit of quantification is 4.3 ng/mL, and upper limit of quantification is 1030 ng/mL. Pharmacokinetic analysis was performed with Watson package (version 6.4.0.04) and Excel spreadsheet (Microsoft Inc., Seattle, USA) using a noncompartmental method (linear trapezoidal rule and linear regression analysis of natural log-transformed plasma concentrations vs time data). Absolute bioavailability (*F*) was calculated from the ratio of average oral to IV (intravenous) dose-normalized plasma AUC (area under curve) values.

**7. In Vivo Pharmacology.** **7.1. 20by Antitumor Activity As Single Agent.** The antitumor activity of compound **20by** was

investigated in female athymic nu/nu mice carrying subcutaneously MDA-MB-436 triple negative BRCA1 mutated breast cancer. When tumors reached an average volume of ~150 mm<sup>3</sup>, mice were randomized into various treatment groups and were treated orally, once a day, for 28 consecutive days, with **20by** (150 mg/kg) or empty vehicle (1% Tween 80 in methocel). Median tumor volume of seven mice per group was determined by caliper and was plotted over time to monitor tumor growth (first day of treatment is day 21).

**7.2. 20by Antitumor Activity in Combination with Temozolomide (TMZ).** In a combination study with Temozolomide, **20by** was administered to male athymic nu/nu mice carrying subcutaneously implanted Capan-1 pancreatic cancer cells, orally once daily for 12 days at the dose of 100 mg/kg, starting on day 9. Temozolomide was administered in glucosate at a dosage of 50 mg/kg for 5 days starting from day 11.

**8. In Vivo Pharmacodynamics.** Tumors of animals treated with a single oral administration of **20by** (100 mg/kg) were harvested at 2, 4, 8, and 24 h, homogenized in PBS, and extracted with lysis buffer. Levels of PAR in the tumor lysates were determined by ELISA. Plates were first coated with anti-PAR monoclonal antibody (Tulip) for 2 h at 37 °C and then washed with PBS 0.1% Tween 20. After blocking, 10 mg of tumor lysates were added to the plate in triplicate and left overnight at 4 °C in PBS 2% BSA and 0.5% SDS. The day after the plates were washed and the polyclonal primary antibody, anti-PAR (Trevigen) was added, diluted 1:2000 in PBS 2% BSA and mouse serum 1:500. Two hours later, the plates were washed with PBS 0.1% Tween 20 and incubated with the secondary antibody anti-HRP (Amersham) diluted 1:1000 in the same buffer as for the primary antibody. The substrate Supersignal ELISA Pico was then added after washes, and the plates were read at 425 nm.

## ■ ASSOCIATED CONTENT

### § Supporting Information

The Supporting Information is available free of charge on the ACS Publications website at DOI: [10.1021/acs.jmedchem.5b00680](https://doi.org/10.1021/acs.jmedchem.5b00680).

Quantitative assessment of the intramolecular hydrogen bond strength of selected isoindolinones; detailed kinetic parameters and kinetic analysis of surface plasmon resonance binding assay; experimental details concerning in vitro evaluation of cross species metabolism, cytochrome P450 inhibition, and mielotoxicity of compound **20by** (PDF)

Isoindolinones preliminary SAR investigation molecular formula strings (XLS)

### Accession Codes

All structures have been deposited to the Protein Data Bank (PDB) with accession codes: 4ZZX, 4ZZY, 4ZZZ, and 5A00.

## ■ AUTHOR INFORMATION

### Corresponding Author

\*Phone: +39-0331581537. Fax: +39-0331581347. E-mail: [gianluca.papeo@nervianoms.com](mailto:gianluca.papeo@nervianoms.com).

### Present Addresses

¶ For B.F. and F.Z.: College of Life Sciences, University of Dundee, Dow Street, Dundee DD1 5EH, Scotland, UK.

† For M.Y.K.: Institute of Chemistry, St. Petersburg State University, 26 Universitetskyi Prospekt, Peterhof 198504, Russian Federation.

### Notes

The authors declare no competing financial interest.

## ■ ACKNOWLEDGMENTS

We gratefully acknowledge the technical skill and support of the Experimental Therapy Team, the Biochemical Screening Group, and Analytical Chemistry Department of NMS.

## ■ ABBREVIATIONS USED

AD, adenine-ribose; ADME, absorption, distribution, metabolism, excretion; ARTD, ADP-ribosyltransferase diphtheria toxin-like; ATM, ataxia telangiectasia mutated; AUC, area under the plasma concentration versus time curve up to the last detectable concentration; BEI, binding efficiency index; BRCA, breast cancer susceptibility gene; BSA, bovine serum albumine; CD, catalytic domain; CL, plasma clearance;  $C_{\max}$ , maximum plasma concentration; DAPI, 4',6-diamidino-2-phenylindole; DTT, dithiothreitol; EGFR, epidermal growth factor receptor; ELISA, enzyme-linked immunosorbent assay; ER, estrogen receptor; F, oral bioavailability; FBS, fetal bovine serum; FCS, fetal calf serum; FL, full length; HER2, human epidermal growth factor receptor 2; HLM, human liver microsomes; HR, homologous recombination; HRP, horseradish peroxidase; HTS, high-throughput screening; LE, ligand efficiency; MEM, minimum essential medium; MSI, microsatellite instability; NAD<sup>+</sup>, nicotinamide adenine dinucleotide; NAMPT, nicotinamide phosphoribosyltransferase; PAR, poly(ADP-ribose); PARP, poly(ADP-ribose) polymerase; PBS, phosphate buffered saline; PEG, polyethylene glycol; PI3K, phosphatidylinositol-3-kinase; PR, progesterone receptor; PTEN, phosphatase and tensin homologue; RPMI, Roswell Park Memorial Institute (culture medium); SAR, structure–activity relationship; SDS, sodium dodecyl sulfate; SEM, standard error of measurement; SIRT1, sirtuin 1;  $t_{1/2}$ , terminal half-life; TNKS-1, tankyrase-1;  $V_{ss}$ , volume of distribution at steady state

## ■ REFERENCES

- (1) Hottiger, M. O.; Hassa, P. O.; Lüscher, B.; Schüler, H.; Koch-Nolte, F. Toward a unified nomenclature for mammalian ADP-ribosyltransferases. *Trends Biochem. Sci.* **2010**, *35*, 208–219.
- (2) Krishnakumar, R.; Kraus, W. L. The PARP side of the nucleus: molecular actions, physiological outcomes, and clinical targets. *Mol. Cell* **2010**, *39*, 8–24.
- (3) (a) Yelamos, J.; Farres, J.; Lacuna, L.; Ampurdanes, C.; Martin-Caballero, J. PARP-1 and PARP-2: new players in tumour development. *Am. J. Cancer Res.* **2011**, *1*, 328–346. (b) Ryu, K. W.; Kim, D.-S.; Kraus, W. L. New Facets in the Regulation of Gene Expression by ADP-Ribosylation and Poly(ADP-ribose) Polymerases. *Chem. Rev.* **2015**, *115*, 2453–2481.
- (4) Ferraris, D. V. Evolution of Poly(ADP-ribose) Polymerase-1 (PARP-1) Inhibitors. From concept to clinic. *J. Med. Chem.* **2010**, *53*, 4561–4584.
- (5) Curtin, N.; Szabo, C. Therapeutic applications of PARP inhibitors: anticancer therapy and beyond. *Mol. Aspects Med.* **2013**, *34*, 1217–1256.
- (6) (a) Penning, T. D. Small-molecule PARP modulators – Current status and future therapeutic potential. *Curr. Opin. Drug Discovery Dev.* **2010**, *13*, 577–586. (b) Jones, P. Development of poly (ADP-Ribose)polymerase (PARP) inhibitors in oncology. *Annu. Rep. Med. Chem.* **2010**, *45*, 229–243. (c) Kummar, S.; Chen, A.; Parchment, R. E.; Kinders, R. J.; Ji, J.; Tomaszewski, J. E.; Doroshow, J. H. Advances in using PARP inhibitors to treat cancer. *BMC Med.* **2012**, *10*, 25. (d) Curtin, N. J. Poly(ADP-ribose) polymerase (PARP) and PARP inhibitors. *Drug Discovery Today: Dis. Models* **2012**, *9*, e51–e58. (e) Maxwell, K. N.; Domchek, S. M. Cancer treatment according to BRCA1 and BRCA2 mutations. *Nat. Rev. Clin. Oncol.* **2012**, *9*, 520–528. (f) Ström, C. E.; Helleday, T. Strategies for the use of poly(adenosine diphosphate ribose) polymerase (PARP) inhibitors in cancer therapy. *Biomolecules* **2012**, *2*, 635–649. (g) Davar, D.; Beumer, J. H.; Hamieh, L.; Tawbi, H. Role of PARP inhibitors in cancer biology and therapy. *Curr. Med. Chem.* **2012**, *19*, 3907–3921. (h) Papeo, G.; Casale, E.; Montagnoli, A.; Cirla, A. PARP inhibitors in cancer therapy: an update. *Expert Opin. Ther. Pat.* **2013**, *23*, 503–514. (i) Ekblad, T.; Camaioni, E.; Schüler, H.; Macchiarulo, A. PARP inhibitors: polypharmacology vs selective inhibition. *FEBS J.* **2013**, *280*, 3563–3575.
- (7) (a) Bryant, H. E.; Schultz, N.; Thomas, H. D.; Parker, K. M.; Flower, D.; Lopez, E.; Kyle, S.; Meuth, M.; Curtin, N. J.; Helleday, T. Specific killing of BRCA2-deficient tumours with inhibitors of poly(ADP-ribose) polymerase. *Nature* **2005**, *434*, 913–917. (b) Farmer, H.; McCabe, N.; Lord, C. J.; Tutt, A. N.; Johnson, D. A.; Richardson, T. B.; Santarosa, M.; Dillon, K. J.; Hickson, I.; Knights, C.; Martin, N. M.; Jackson, S. P.; Smith, G. C.; Ashworth, A. Targeting the DNA repair defect in BRCA mutant cells as a therapeutic strategy. *Nature* **2005**, *434*, 917–921.
- (8) (a) Ibrahim, Y. H.; García-García, C.; Serra, V.; He, L.; Torres-Lockhart, K.; Prat, A.; Anton, P.; Cozar, P.; Guzmán, M.; Grueso, J.; Rodríguez, O.; Calvo, M. T.; Aura, C.; Díez, O.; Rubio, I. T.; Pérez, J.; Rodón, J.; Cortés, J.; Ellisen, L. W.; Scaltriti, M.; Baselga, J. PI3K Inhibition impairs BRCA1/2 expression and sensitizes BRCA-proficient triple-negative breast cancer to PARP inhibition. *Cancer Discovery* **2012**, *2*, 1036–1047. (b) Juvekar, A.; Burga, L. N.; Hu, H.; Lunsford, E. P.; Ibrahim, Y. H.; Balmañà, J.; Rajendran, A.; Papa, A.; Spencer, K.; Lyssiotis, C. A.; Nardella, C.; Pandolfi, P. P.; Baselga, J.; Scully, R.; Asara, J. M.; Cantley, L. C.; Wulf, G. M. Combining a PI3K inhibitor with a PARP inhibitor provides an effective therapy for a mouse model of BRCA1-related breast cancer. *Cancer Discovery* **2012**, *2*, 1048–1063.
- (9) Bajrami, I.; Kigozi, A.; Van Weverwijk, A.; Brough, R.; Frankum, J.; Lord, C. J.; Ashworth, A. Synthetic lethality of PARP and NAMPT inhibition in triple-negative breast cancer cells. *EMBO Mol. Med.* **2012**, *4*, 1087–1096.
- (10) Nowsheen, S.; Cooper, T.; Stanley, J. A.; Yang, E. S. Synthetic lethal interactions between EGFR and PARP inhibition in human triple negative breast cancer cells. *PLoS One* **2012**, *7*, e46614.
- (11) (a) Mendes-Pereira, A. M.; Martin, S. A.; Brough, R.; McCarthy, A.; Taylor, J. R.; Kim, J.-S.; Waldman, T.; Lord, C. J.; Ashworth, A. Synthetic lethal targeting of PTEN mutant cells with PARP inhibitors. *EMBO Mol. Med.* **2009**, *1*, 315–322. (b) Garcia-Cao, I.; Song, M. S.; Hobbs, R. M.; Laurent, G.; Giorgi, C.; de Boer, V. C.; Anastasiou, D.; Ito, K.; Sasaki, A. T.; Rameh, L.; Carracedo, A.; Vander Heiden, M. G.; Cantley, L. C.; Pinton, P.; Haigis, M. C.; Pandolfi, P. P. Systemic elevation of PTEN induces a tumor-suppressive metabolic state. *Cell* **2012**, *149*, 49–62.
- (12) Williamson, C. T.; Muzik, H.; Turhan, A. G.; Zamò, A.; O'Connor, M. J.; Bebb, D. G.; Lees-Miller, S. P. ATM deficiency sensitizes mantle cell lymphoma cells to poly(ADP-ribose) polymerase-1 inhibitors. *Mol. Cancer Ther.* **2010**, *9*, 347–357.
- (13) Vilar, E.; Gruber, S. B. Microsatellite instability in colorectal cancer—the stable evidence. *Nat. Rev. Clin. Oncol.* **2010**, *7*, 153–162.
- (14) Brenner, J. C.; Feng, F. Y.; Han, S.; Patel, S.; Goyal, S. V.; Bou-Maroun, L. M.; Liu, M.; Lonigro, R.; Prensner, J. R.; Tomlins, S. A.; Chinnaiyan, A. M. PARP-1 inhibition as a targeted strategy to treat Ewing's sarcoma. *Cancer Res.* **2012**, *72*, 1608–1613.
- (15) Penning, T. D.; Zhu, G. D.; Gandhi, V. B.; Gong, J.; Liu, X.; Shi, Y.; Klinghofer, V.; Johnson, E. F.; Donawho, C. K.; Frost, D. J.; Bontcheva-Diaz, V.; Bouska, J. J.; Osterling, D. J.; Olson, A. M.; Marsh, K. C.; Luo, Y.; Giranda, V. L. Discovery of the poly-(ADP-ribose) polymerase (PARP) inhibitor 2-[*R*]-2-methylpyrrolidin-2-yl]-1H-benzimidazole-4-carboxamide (ABT-888) for the treatment of cancer. *J. Med. Chem.* **2009**, *52*, 514–523.
- (16) (a) Jones, P.; Altamura, S.; Boueres, J.; Ferrigno, F.; Fonsi, M.; Giomini, C.; Lamartina, S.; Monteagudo, E.; Ontoria, J. M.; Orsala, M. V.; Palumbi, M. C.; Pesci, S.; Roscilli, G.; Scarcelli, R.; Schultz-Fademrecht, C.; Toniatti, C.; Rowley, M. Discovery of 2-[*4*-[(3*S*)-piperidin-3-yl]phenyl]-2H-indazolo-7-carboxamide (MK-4827): a novel oral poly(ADP-ribose)polymerase (PARP) inhibitor efficacious in BRCA-1 and -2 mutant tumors. *J. Med. Chem.* **2009**, *52*, 7170–7185. (b) Jones, P.; Wilcoxon, K.; Rowley, M.; Toniatti, C. Niraparib: a poly(ADP-ribose) polymerase (PARP) inhibitor for the treatment of tumors with defective homologous recombination. *J. Med. Chem.* **2015**, *58*, 3302–3314.

- (17) Thomas, H. D.; Calabrese, C. R.; Batey, M. A.; Canan, S.; Hostomsky, Z.; Kyle, S.; Maegley, K. A.; Newell, D. R.; Skalitzky, D.; Wang, L.-Z.; Webber, S. E.; Curtin, N. J. Preclinical selection of a novel poly(ADP-ribose) polymerase inhibitor for clinical trial. *Mol. Cancer Ther.* **2007**, *6*, 945–956.
- (18) Menear, K. A.; Adcock, C.; Boulter, R.; Cockcroft, X. L.; Copsey, L.; Cranston, A.; Dillon, K. J.; Drzewiecki, J.; Garman, S.; Gomez, S.; Javaid, H.; Kerrigan, F.; Knights, C.; Lau, A.; Loh, V. M., Jr.; Matthews, I. T.; Moore, S.; O'Connor, M. J.; Smith, G. C.; Martin, N. M. 4-[3-(4-Cyclopropanecarbonylpiperazine-1-carbonyl)-4-fluorobenzyl]-2H-phthalazin-1-one: a novel bioavailable inhibitor of poly(ADP-ribose) polymerase-1. *J. Med. Chem.* **2008**, *51*, 6581–6591.
- (19) (a) Shen, Y.; Rehman, F. L.; Feng, Y.; Boshuizen, J.; Bajrami, L.; Elliott, R.; Wang, B.; Lord, C. J.; Post, L. E.; Ashworth, A. BMN673, a novel and highly potent PARP1/2 inhibitor for the treatment of human cancers with DNA repair deficiency. *Clin. Cancer Res.* **2013**, *19*, 5003–5015. (b) Shen, Y.; Aoyagi-Scharber, M.; Wang, B. Trapping Poly(ADP-Ribose) Polymerase. *J. Pharmacol. Exp. Ther.* **2015**, *353*, 446–457.
- (20) Wahlberg, E.; Karlberg, T.; Kouznetsova, E.; Markova, N.; Macchiarulo, A.; Thorsell, A.-G.; Pol, E.; Frostell, A.; Ekblad, T.; Öncü, D.; Kull, B.; Robertson, G. M.; Pellicciari, R.; Schüller, H.; Weigelt, J. Family-wide chemical profiling and structural analysis of PARP and tankyrase inhibitors. *Nat. Biotechnol.* **2012**, *30*, 283–288.
- (21) Papeo, G.; Avanzi, N.; Bettoni, S.; Leone, A.; Paolucci, M.; Perego, R.; Quartieri, F.; Riccardi-Sirtori, F.; Thieffine, S.; Montagnoli, A.; Lupi, R. Insights into PARP inhibitors selectivity using fluorescence polarization and surface plasmon resonance binding assays. *J. Biomol. Screening* **2014**, *19*, 1212–1219.
- (22) Yélamos, J.; Schreiber, V.; Dantzer, F. Toward specific functions of poly(ADP-ribose) polymerase-2. *Trends Mol. Med.* **2008**, *14*, 169–178.
- (23) Antolin, A. A.; Mestres, J. Linking off-target kinase pharmacology to the differential cellular effects observed among PARP inhibitors. *Oncotarget* **2014**, *5*, 3023–3028.
- (24) Farrés, J.; Llacuna, L.; Martin-Caballero, J.; Martínez, C.; Lozano, J. J.; Ampurdanés, C.; López-Contreras, A. J.; Florensa, L.; Navarro, J.; Ottina, E.; Dantzer, F.; Schreiber, V.; Villunger, A.; Fernández-Capetillo, O.; Yélamos, J. PARP-2 sustains erythropoiesis in mice by limiting replicative stress in erythroid progenitors. *Cell Death Differ.* **2015**, *22*, 1144–1157.
- (25) Goldberg, M. S.; Xing, D.; Ren, Y.; Orsulic, S.; Bhatia, S. N.; Sharp, P. A. Nanoparticle-mediated delivery of siRNA targeting Parp1 extends survival of mice bearing tumors derived from Brca1-deficient ovarian cancer cells. *Proc. Natl. Acad. Sci. U. S. A.* **2011**, *108*, 745–750.
- (26) (a) Ishida, J.; Yamamoto, H.; Kido, Y.; Kamijo, K.; Murano, K.; Miyake, H.; Ohkubo, M.; Kinoshita, T.; Warizaya, M.; Iwashita, A.; Miura, K.; Matsuo, N.; Hattori, K. Discovery of potent and selective PARP-1 and PARP-2 inhibitors: SBDD analysis via a combination of X-ray structural study and homology modeling. *Bioorg. Med. Chem.* **2006**, *14*, 1378–1390. (b) Hattori, K.; Kido, Y.; Yamamoto, H.; Ishida, J.; Iwashita, A.; Miura, K. Rational design of conformationally restricted quinazolinone inhibitors of poly(ADP-ribose)polymerase. *Bioorg. Med. Chem. Lett.* **2007**, *17*, 5577–5581.
- (27) Eltze, T.; Boer, R.; Wagner, T.; Weinbrenner, S.; McDonald, M. C.; Thiemermann, C.; Bürkle, A.; Klein, T. Imidazoquinolinone, imidazopyridine, and isoquinolindione derivatives as novel and potent inhibitors of the poly(ADP-ribose) polymerase (PARP): a comparison with standard PARP inhibitors. *Mol. Pharmacol.* **2008**, *74*, 1587–1598.
- (28) (a) Varlamov, A. V.; Boltukhina, E. V.; Zubkov, F. I.; Sidorenko, N. V.; Chernyshev, A. I.; Grudinin, D. G. Preparative synthesis of 7-carboxy-2-R-isoindol-1-ones. *Chem. Heterocycl. Compd.* **2004**, *40*, 22–28. (b) Medimagh, R.; Marque, S.; Prim, D.; Chatti, S. 5-Amino-2-furylmethylamines – appealing precursors of amino-isoindolinones? *Synthesis* **2010**, *2010*, 770–774. (c) Ball, M.; Boyd, A.; Churchill, G.; Cuthbert, M.; Drew, M.; Fielding, M.; Ford, G.; Frodsham, L.; Golden, M.; Leslie, K.; Lyons, S.; McKeever-Abbas, B.; Stark, A.; Tomlin, P.; Gottschling, S.; Hajar, A.; Jiang, J.-I.; Lo, J.; Suchozak, B. Isoindolone formation via intramolecular Diels-Alder reaction. *Org. Process Res. Dev.* **2012**, *16*, 741–747. (d) Zaytsev, V. P.; Mikhailova, N. M.; Airyan, I. K.; Galkina, E. V.; Golubev, V. D.; Nikitina, E. V.; Zubkov, F. I.; Varlamov, A. V. Cycloaddition of furfurylamines to maleic anhydride and its substituted derivatives. *Chem. Heterocycl. Compd.* **2012**, *48*, 505–513. (e) De Cesco, S.; Deslandes, S.; Therrien, E.; Levan, D.; Cueto, M.; Schmidt, R.; Cantin, L.-D.; Mittermaier, A.; Juillerat-Jeanneret, L.; Moitessier, N. Virtual screening and computational optimization for the discovery of covalent prolyl oligopeptidase inhibitors with activity in human cells. *J. Med. Chem.* **2012**, *55*, 6306–6315.
- (29) (a) Zubkov, F. I.; Boltukhina, E. V.; Turchin, K. F.; Borisov, R. S.; Varlamov, A. V. New synthetic approach to substituted isoindolo[2,1-a]quinoline carboxylic acids via intramolecular Diels-Alder reaction of 4-(N-furyl-2)-4-arylaminoctenes-1 with maleic anhydride. *Tetrahedron* **2005**, *61*, 4099–4113. (b) Boltukhina, E. V.; Zubkov, F. I.; Nikitina, E. V.; Varlamov, A. V. Novel approach to isoindolo[2,1-a]quinolines: synthesis of 1- and 3-halo-substituted 11-oxo-5,6,6a,11-tetrahydroisoindolo[2,1-a]quinoline-10-carboxylic acids. *Synthesis* **2005**, *2005*, 1859–1875.
- (30) Gandhi, V. B.; Luo, Y.; Liu, X.; Shi, Y.; Klinghofer, V.; Johnson, E. F.; Park, C.; Giranda, V. L.; Penning, T. D.; Zhu, G.-D. Discovery and SAR of substituted 3-oxoisooindoline-4-carboxamides as potent inhibitors of poly(ADP-ribose) polymerase (PARP) for the treatment of cancer. *Bioorg. Med. Chem. Lett.* **2010**, *20*, 1023–1026.
- (31) Mei, T.-S.; Giri, R.; Maugel, N.; Yu, J.-Q. Pd<sup>II</sup>-Catalyzed monoselective *ortho* halogenation of C-H bonds assisted by counter cations: a complementary method to directed *ortho* lithiation. *Angew. Chem., Int. Ed.* **2008**, *47*, 5215–5219.
- (32) Jagtap, P. G.; Southan, G. J.; Baloglu, E.; Ram, S.; Mabley, J. G.; Marton, A.; Salzman, A.; Szabo, C. The discovery and synthesis of novel adenosine substituted 2,3-dihydro-1H-isoindol-1-ones: potent inhibitors of poly(ADP-ribose) polymerase-1 (PARP-1). *Bioorg. Med. Chem. Lett.* **2004**, *14*, 81–85.
- (33) Papeo, G. M. E.; Anatolieva Busel, A.; Khvat, A.; Krasavin, M. Y.; Forte, B.; Zuccotto, F. 3-Oxo-2,3-dihydro-1H-isoindole-4-carboxamides as PARP inhibitors. Patent WO2011/006794, 2011.
- (34) Kim, E. S.; Lee, H. S.; Kim, S. H.; Kim, J. N. An efficient InCl<sub>3</sub>-catalyzed hydration of nitriles to amides: acetaldoxime as an effective water surrogate. *Tetrahedron Lett.* **2010**, *51*, 1589–1591.
- (35) Li, J.-H.; Zhang, J.; Jackson, P. F.; Maclin, K. M. Compounds, methods and pharmaceutical compositions for treating neural or cardiovascular tissue damage. U.S. Patent 6306889, 2001.
- (36) (a) Abad-Zapatero, C. Ligand efficiency indices for effective drug discovery. *Expert Opin. Drug Discovery* **2007**, *2*, 469–488. (b) Abad-Zapatero, C.; Perićić, O.; Wass, J.; Bento, A. P.; Overington, J.; Al-Lazikani, B.; Johnson, M. E. Ligand efficiency indices for an effective mapping of chemico-biological space: the concept of an atlas-like representation. *Drug Discovery Today* **2010**, *15*, 804–811.
- (37) (a) Lord, A.-M.; Mahon, M. F.; Lloyd, M. D.; Threadgill, M. D. Design, synthesis and evaluation in vitro of quinoline-8-carboxamides, a new class of poly(adenosine-diphosphate-ribose)polymerase-1 (PARP-1) inhibitor. *J. Med. Chem.* **2009**, *52*, 868–877. (b) Gorobets, N. Y.; Yermolayev, S. A.; Gurley, T.; Gurinov, A. A.; Tolstoy, P. M.; Shenderovich, I. G.; Leadbeater, N. E. Difference between <sup>1</sup>H NMR signals of primary amide protons as a simple spectral index of the amide intramolecular hydrogen bond strength. *J. Phys. Org. Chem.* **2012**, *25*, 287–295.
- (38) Abraham, M. H.; Abraham, R. J.; Acree, W. E., Jr.; Aliev, A. E.; Leo, A. J.; Whaley, W. L. An NMR Method for the Quantitative Assessment of Intramolecular Hydrogen Bonding; Application to Physicochemical, Environmental, and Biochemical Properties. *J. Org. Chem.* **2014**, *79*, 11075–11083.
- (39) As the *K*<sub>D</sub> sensitivity limit of the fluorescence polarization assay used to evaluate the biochemical potency of the inhibitors is 0.030 μM, a *K*<sub>D</sub> ≥ 2 μM threshold against PARP-2 was introduced to evaluate the selectivity of the compounds that reach the aforementioned assay limit against PARP-1.
- (40) The 4,4-difluorocyclohexyl moiety was chosen in light of its purported superior metabolic stability compared to the corresponding

unsubstituted cyclohexyl derivative. See, for example: (a) Dorr, P.; Westby, M.; Dobbs, S.; Griffin, P.; Irvine, B.; Macartney, M.; Mori, J.; Rickett, G.; Smith-Burchell, C.; Napier, C.; Webster, R.; Armour, D.; Price, D.; Stammen, B.; Wood, A.; Perros, M. Maraviroc (UK-427,857), a Potent, Orally Bioavailable, and Selective Small-Molecule Inhibitor of Chemokine Receptor CCR5 with Broad-Spectrum Anti-Human Immunodeficiency Virus Type 1 Activity. *Antimicrob. Agents Chemother.* **2005**, *49*, 4721–4732. (b) Kuduk, S. D.; Chang, R. K.; DiPardo, R. M.; Di Marco, C. N.; Murphy, K. L.; Ransom, R. W.; Reiss, D. R.; Tang, C.; Prueksaritanont, T.; Pettibone, D. J.; Bock, M. G. Bradykinin B<sub>1</sub> receptor antagonists: An  $\alpha$ -hydroxy amide with an improved metabolism profile. *Bioorg. Med. Chem. Lett.* **2008**, *18*, 5107–5110.

(41) Robichaud, J.; Black, W. C.; Thérien, M.; Paquet, J.; Oballa, R. M.; Bayly, C. I.; McKay, D. J.; Wang, Q.; Isabel, E.; Léger, S.; Mellon, C.; Kimmel, D. B.; Wesolowski, G.; Percival, M. D.; Massé, F.; Desmarais, S.; Falgueyret, J.-P.; Crane, S. N. Identification of a nonbasic, nitrile-containing cathepsin K inhibitor (MK-1256) that is efficacious in a monkey model of osteoporosis. *J. Med. Chem.* **2008**, *51*, 6410–6420.

(42) Boudra, M. T.; Bolin, C.; Chiker, S.; Fouquin, A.; Zaremba, T.; Vaslin, L.; Biard, D.; Cordelières, F. P.; Mégnin-Chanet, F.; Favaudon, V.; Fernet, M.; Pennaneach, V.; Hall, J. PARP-2 depletion results in lower radiation cell survival but cell line specific differences in poly(ADP-ribose) levels. *Cell. Mol. Life Sci.* **2015**, *72*, 1585–1597.

(43) Karlberg, T.; Hammarström, M.; Schütz, P.; Svensson, L.; Schüler, H. Crystal Structure of the Catalytic Domain of Human PARP2 in Complex with PARP Inhibitor ABT-888. *Biochemistry* **2010**, *49*, 1056–1058.

(44) Colombo, M.; Sirtori, F. R.; Rizzo, V. A fully automated method for accurate mass determination using high-performance liquid chromatography with a quadrupole/orthogonal acceleration time-of-flight mass spectrometer. *Rapid Commun. Mass Spectrom.* **2004**, *18*, 511–517.

(45) Felder, E. R.; Badari, A.; Disingrini, T.; Mantegani, S.; Orrenius, C.; Avanzi, N.; Isacchi, A.; Salom, B. The generation of purinome-targeted libraries as a means to diversify ATP-mimetic chemical classes for lead finding. *Mol. Diversity* **2012**, *16*, 27–51.

(46) GraphPad Prism; GraphPad Software, Inc.: 7825 Fay Avenue, Suite 230 La Jolla, CA 92037 USA.

(47) Leslie, A. G. W. Integration of macromolecular diffraction data. *Acta Crystallogr., Sect. D: Biol. Crystallogr.* **1999**, *55*, 1696–1702.

(48) Collaborative Computational Project, Number 4. The CCP4 suite: programs for protein crystallography. *Acta Crystallogr., Sect. D: Biol. Crystallogr.* **1994**, *50*, 760–763.

(49) Murshudov, G. N.; Vagin, A. A.; Dodson, E. J. Refinement of Macromolecular Structures by the Maximum-Likelihood Method. *Acta Crystallogr., Sect. D: Biol. Crystallogr.* **1997**, *53*, 240–255.

(50) Emsley, P.; Cowtan, K. Coot: model-building tools for molecular graphics. *Acta Crystallogr., Sect. D: Biol. Crystallogr.* **2004**, *60*, 2126–2132.

(51) Beria, I.; Ballinari, D.; Bertrand, J. A.; Borghi, D.; Bossi, R. T.; Brasca, M. G.; Cappella, P.; Caruso, M.; Ceccarelli, W.; Ciavolella, A.; Cristiani, C.; Croci, V.; De Ponti, A.; Fachin, G.; Ferguson, R. D.; Lansen, J.; Moll, J. K.; Pesenti, E.; Posteri, H.; Perego, R.; Rocchetti, M.; Storici, P.; Volpi, D.; Valsasina, B. Identification of 4,5-dihydro-1*H*-pyrazolo[4,3-*h*]quinazoline derivatives as a new class of orally and selective polo-like kinase 1 inhibitors. *J. Med. Chem.* **2010**, *53*, 3532–3551.

(52) Kerns, E. H.; Di, L.; Petusky, S.; Farris, M.; Ley, R.; Jupp, P. Combined application of parallel artificial membrane permeability assay and Caco-2 permeability assays in drug discovery. *J. Pharm. Sci.* **2004**, *93*, 1440–1453.